

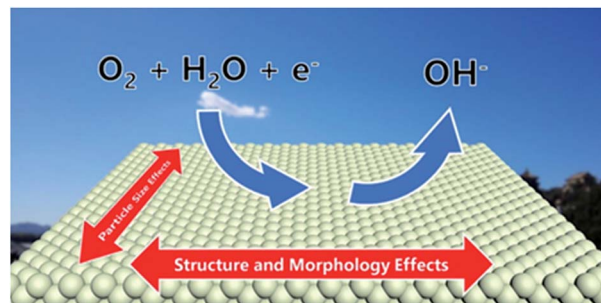
## REVIEW

1

**A comprehensive review of Pt electrocatalysts for the oxygen reduction reaction: Nanostructure, activity, mechanism and carbon support in PEM fuel cells**

Sheng Sui,\* Xiaoying Wang, Xintong Zhou, Yuehong Su, Saffa Riffat and Chang-jun Liu\*

This paper reviews progress in studies of the mechanism, nanostructure, size effect and carbon supports of Pt electrocatalysts for the ORR.



Please check this proof carefully. **Our staff will not read it in detail after you have returned it.**

Translation errors between word-processor files and typesetting systems can occur so the whole proof needs to be read. Please pay particular attention to: tabulated material; equations; numerical data; figures and graphics; and references. If you have not already indicated the corresponding author(s) please mark their name(s) with an asterisk. Please e-mail a list of corrections or the PDF with electronic notes attached - do not change the text within the PDF file or send a revised manuscript. Corrections at this stage should be minor and not involve extensive changes. All corrections must be sent at the same time.

**Please bear in mind that minor layout improvements, e.g. in line breaking, table widths and graphic placement, are routinely applied to the final version.**

We will publish articles on the web as soon as possible after receiving your corrections; **no late corrections will be made.**

Please return your **final** corrections, where possible within **48 hours** of receipt by e-mail to: materialsA@rsc.org

# 1 Queries for the attention of the authors 1

Journal: Journal of Materials Chemistry A

5 Paper: c6ta08580f 5

Title: A comprehensive review of Pt electrocatalysts for the oxygen reduction reaction: Nanostructure, activity, mechanism and carbon support in PEM fuel cells

10 Editor's queries are marked like this... **1**, and for your convenience line numbers are inserted like this... 5 10

Please ensure that all queries are answered when returning your proof corrections so that publication of your article is not delayed.

15 Query Reference	Query	Remarks
20 1	For your information: You can cite this article before you receive notification of the page numbers by using the following format: (authors), J. Mater. Chem. A, (year), DOI: 10.1039/c6ta08580f.	
25 2	Biography text is limited to 100 words to fit the space available. I have shortened the entries for Dr Sui and Professor Liu - please check.	
30 3	Please carefully check the spelling of all author names. This is important for the correct indexing and future citation of your article. No late corrections can be made.	
35 4	Please check that the GA text fits within the allocated space indicated on the front page of the proof. If the entry does not fit between the two horizontal lines, then please trim the text and/or the title.	
40 5	Ref. 32: Can this reference be updated?	

## REVIEW

# A comprehensive review of Pt electrocatalysts for the oxygen reduction reaction: Nanostructure, activity, mechanism and carbon support in PEM fuel cells

Cite this: DOI: 10.1039/c6ta08580f

Sheng Sui,<sup>\*ac</sup> Xiaoying Wang,<sup>a</sup> Xintong Zhou,<sup>b</sup> Yuehong Su,<sup>c</sup> Saffa Riffat<sup>c</sup> and Chang-jun Liu<sup>\*b</sup>

The sluggish rate of the oxygen reduction reaction (ORR) in proton exchange membrane (PEM) fuel cells has been a major challenge. Significantly increasing efforts have been made worldwide towards a highly active ORR catalyst with high durability. Among all the catalysts exploited, Pt electrocatalysts are still the best in terms of a comprehensive evaluation. The investigation of Pt-based ORR catalysts is necessary for a practical ORR catalyst with low Pt content. This paper reviews recent progress in the studies of the mechanism, nanostructure, size effect and carbon supports of Pt electrocatalysts for the ORR. The importance of the size and structure control of Pt ORR catalysts, related with carbon support materials, is indicated. The potential methods for such control are discussed. The progress in theoretical studies and *in situ* catalyst characterization are also discussed. Finally, challenges and future developments are addressed.

Received 3rd October 2016  
Accepted 5th December 2016

DOI: 10.1039/c6ta08580f

www.rsc.org/MaterialsA

<sup>a</sup>Institute of Fuel Cells, Shanghai Jiao Tong University, Shanghai 200240, China.  
E-mail: ssui@sjtu.edu.cn<sup>b</sup>Collaborative Innovation Center of Chemical Science and Engineering, School of Chemical Engineering and Technology, Tianjin University, Tianjin 300072, China.  
E-mail: coronacj@tju.edu.cn<sup>c</sup>Department of Architecture and Built Environment, University of Nottingham, Nottingham NG7 2RD, UK

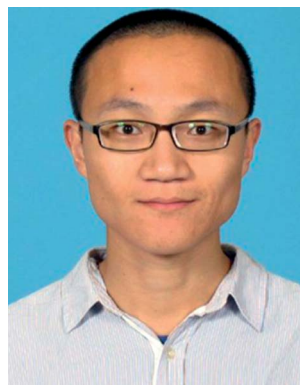
## 1. Introduction

It is generally accepted that fuel cells give an ultimate energy solution because of their high efficiency, zero emission, quiet operation process and unlimited renewable source of reactants.<sup>1–4</sup> Stationary power, transportation and portable power are the three major markets for fuel cell technology. Among various fuel cells, the proton exchange membrane (PEM) fuel



Dr Sheng Sui is an Associate Professor at the Institute of Fuel Cells of Shanghai Jiao Tong University (China). He is now a Marie Skłodowska-Curie fellow at the Department of Architecture and Built Environment at the University of Nottingham (UK). He has nearly 20 years' research experience in the fields of proton exchange membrane fuel cells (PEMFCs) and molten carbonate fuel cells.

He currently focuses on electrocatalysts, electrode structures and membrane electrode assemblies in PEMFCs. He also investigates coal-slurry electrolysis for hydrogen production, regenerative fuel cells for energy storage, and low-Pt-loading fuel cells for cogeneration applications in buildings.



Xiaoying Wang is currently a PhD candidate at the Institute of Fuel Cells, Shanghai Jiao Tong University (China). He has participated in several research projects on the theoretical analysis and syntheses of novel electrocatalysts for the oxygen reduction reaction and optimization of membrane electrode assemblies in PEMFCs.

cell with the advantages of low operating temperature, quick starting and a compact stack, has attracted much attention worldwide. A recent landmark event in the fuel cell arena is Toyota's launch of its hydrogen fuel cell vehicle "Mirai" at the Los Angeles Auto Show, November 2014. This is one of the first such mass-market vehicles sold commercially.<sup>5</sup> This has given rise to a new tide in fuel cell research. However, the sluggish rate of the oxygen reduction reaction (ORR) at the cathode is still a major challenge in the research and development of PEM fuel cells. Platinum (Pt) is the best single metal electrocatalyst for the ORR with high activity and durability in acid,<sup>6</sup> while its ORR rate is ~5 orders of magnitude slower than the hydrogen oxidation reaction at the anode. Consequently, the cathode of a PEM fuel cell typically contains 80–90% of the total Pt in the stack. Due to the scarcity and high cost of platinum, the target total Pt-loading (anode + cathode) is required to be below 0.125 mg cm<sup>-2</sup> in 2017, according to the US Department of Energy (DOE), compared with present status of ~0.4 mg cm<sup>-2</sup> or more

used on cathodes.<sup>7</sup> Reducing the Pt loading of the cathode without a loss in performance is the subject of most electrocatalytic studies.<sup>8,9</sup> Until now, Pt-based electrocatalysts have been the only choice in practical PEM fuel cells. Although many efforts towards Pt-free electro-catalysts, like non-precious transition metals, metal nitrides and nanoscale carbon-based metal-free electrocatalysts are under investigation, it is rather difficult to presume that these catalysts will be commercially available for the fuel cell industry, due to the poor stability and limited performance of these kinds of catalysts.<sup>9,10</sup> Most emerging approaches still focus on controlling the surface structure and surface electronic state (or composition) of platinum nanoparticles (NPs) to achieve higher ORR activity with less Pt. Some new synthetic routes have delivered such "designer nanoparticles".<sup>7,11</sup>

As shown in Fig. 1, Pt-based electrocatalysts can be classed into three main groupings: pure platinum, platinum alloys and core-shell platinum structures, which show different activity



*Xintong Zhou is currently a PhD candidate at Tianjin University. He received his bachelor's degree in 2011 and master's degree in 2014 from Tianjin University. He has published one paper in Frontiers of Chemical Science and Engineering on porous zinc oxide nanostructures.*



*Professor Yaffa Riffat, the President of the World Society of Sustainable Energy Technologies and the Head of Architecture, Energy & Environment Research Group, Department of Architecture & Built Environment, University of Nottingham (UK), is one of the leading experts in sustainable technologies/eco-buildings. He has extensive expertise in the field of the "Creative Energy Home"*

*(Fuel cell integrated CHP), energy storage, tri-generation (combined power, heating and cooling), advanced heat transfer enhancement methods and fluid flow modelling. He holds 30 international patents and published over 500 peer-reviewed papers.*



*Dr Yuehong Su is an Associate Professor in Energy and Building at the Department of Architecture and Built Environment, University of Nottingham, UK. He has wide research interests in fuel cells, air conditioning, adsorption/absorption/ejector cooling, energy efficiency, heat storage, combined heat & power, day-lighting, solar concentration, CFD modelling and building simulation. He has published over 80 papers in refereed journals and conferences.*



*Prof. Chang-jun Liu has published more than 200 papers. He was included in the list of highly cited Chinese authors (Chemical Engineering, 2014–2015) by Elsevier. He has made more than 40 speeches at international conferences. He served as the 2010 Program Chair of the Fuel Chemistry Division of the American Chemical Society and Chair of the 10th International Conference on CO<sub>2</sub> Utilization.*

*He was an advisory board member of Energy & Environmental Science, and board member of Greenhouse Gases: Science & Technology, Applied Catalysis B, Journal of Energy Chemistry, Journal of CO<sub>2</sub> Utilization and Chinese Journal of Catalysis.*

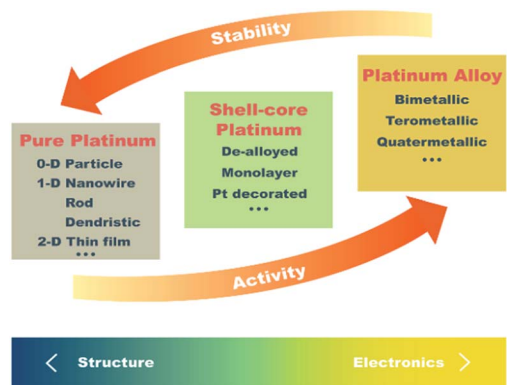


Fig. 1 Groupings of Pt-based electrocatalysts for ORR in PEM fuel cells.

and stability after their controlling structure/geometry and electronic state. Alloying Pt with other metals can vary the bond strength between the electrocatalyst and the ORR intermediates, leading to a higher ORR catalytic activity. It can also help the cost effectiveness of a fuel cell by reducing the total Pt content in the catalyst. Beside the enormous number of binary alloy catalysts for ORR explored for several decades, the ternary, quaternary and quinary alloys have now been investigated in the past few years.<sup>12–16</sup> Stamenkovic *et al.*<sup>17</sup> demonstrated that the Pt<sub>3</sub>Ni (111) surface possesses 90-fold more activity than the current commercial Pt/C catalysts for PEM fuel cells. Pt<sub>x</sub>Gd NPs exhibited an outstanding activity of 3.6 A mg<sup>-1</sup> Pt at 0.9 V RHE in acid half cells, a little lower than Pt<sub>3</sub>Ni (111).<sup>14</sup> However, Pt alloys are thermodynamically unstable under fuel cell conditions. The transition metal alloyed with platinum tends to dissolve into the electrolyte *via* a process known as dealloying. The leakage level (or Pt enrichment) and the thickness of the dealloyed region vary with different alloys, preparation techniques and electrochemical treatments.<sup>18,19</sup> Although some Pt alloy catalysts with advanced nanostructures have shown remarkable activity, the dissolution of metals, including Pt and alloyed base metals, in fuel cell operation environments could cause catalyst degradation and pollute electrolyte membranes. This still remains an issue. Another issue may be the low retention of the active catalyst nanostructure during fuel cell operation.<sup>16</sup>

The idea of a core-shell structure is to improve the utilization of Pt atoms by depositing or forming a thin Pt-based shell (several atom layers) around a less expensive core, such as Pd-, Ru-, and Re-based NPs.<sup>5</sup> The Pt “shell” could be in different forms, like: a Pt-rich surface layer by electrochemical de-alloying<sup>20</sup> or annealing<sup>21</sup> or acid leaching;<sup>14</sup> a Pt overlayer by seed-based chemical reduction;<sup>22</sup> and a Pt monolayer by underpotential deposition.<sup>23,24</sup> Chung *et al.*<sup>25</sup> demonstrated that the ORR of the NPs is significantly affected by their subsurface composition rather than their bulk composition. An appropriate Pt-skin thickness and modulated subsurface structure induces geometric and electronic effects that enhance the ORR activity.<sup>9</sup> However, the surface segregation, the composition change for Pt alloys and insufficient Pt surface coverage for

the Pt monolayer affect the stability and activity of these catalysts.<sup>9,21</sup>

With the advances in *in situ* characterization techniques,<sup>13,26–29</sup> significant progress in Pt catalysts with tailored structures have been made. Electrochemical reactions with selectivity tuning become possible with an atomically dispersed platinum catalyst.<sup>30</sup> As Pt-based electro-catalysts, pure platinum, platinum alloys and core-shell structures have their own advantages and disadvantages. Facile crystallographic control and relative chemical inertness give pure Pt distinct activity and stability, while the surface electronic structure (the d-band center) of Pt can be accurately modified by alloying with 3d-transition metals.<sup>27</sup> Shell-core Pt NPs show the most significant potential as ORR catalysts because of their balance between activity and stability.<sup>21,31</sup> Pt is the benchmark for guiding the development of new highly active and durable ORR catalysts. It remains a topic of foremost importance in fundamental electrochemistry and applied electrochemical materials science.<sup>32</sup> In the present review, we aim to summarize the recent progress in the studies of ORR theory, the influence of carbon support materials, and the structure and size effects of Pt NPs. Challenges and future developments will be addressed at end of the review.

## 2. ORR theory studies

Catalysis is determined at the atomic scale. Its rational understanding usually requires a knowledge of the atomic and electronic structures of the catalyst.<sup>33</sup> The mechanism of the electrochemical reduction of oxygen is rather complicated, including multi-electron transfer processes through several elementary steps with various intermediate species. It is affected by the reaction temperature, oxygen partial pressure and potential.<sup>34</sup> There is still no overwhelming consensus on the ORR mechanism due to the lack of suitable experimental validation techniques, which can identify accurately the composition and coverage of surface intermediates formed during the reaction.<sup>34,35</sup> To some extent, experimental characterization techniques<sup>27,29,36</sup> and computational catalytic studies<sup>33,37</sup> have been adopted to depict the ORR mechanism and catalyst design in recent years.

### 2.1 Reaction pathway

It is generally accepted that ORR proceeds through either a “direct” four-electron pathway or a “series” of two-electron processes, suggested by Wroblowa *et al.*<sup>38</sup> The four-electron reaction, a so-called “direct” manner, has been unanimously recognized as the favoured pathway: (a) it has no peroxide species that contribute to certain degradation mechanisms of the electrode and the electrolyte membrane; and (b) there are higher operating potentials and current efficiency in the PEM fuel cells.<sup>39</sup> However, the “series” or “indirect” two-electron reaction is possible on Pt particles in sulfuric acid, based on experimental results and a theoretical model, which is unfavoured as the intermediate H<sub>2</sub>O<sub>2</sub> would reduce the effective electron-transfer number ( $\eta_{\text{eff}}$ ) of the ORR and may also

significantly increase the degradation rate of any organic materials presented, for example, the proton conducting solid polymer electrolyte.<sup>40</sup>

Density functional theory (DFT), using the electronic density to evaluate the energy of a system, can calculate the electronic energy of any configuration of nuclei and electrons of the catalyst, which provides a representation of the energy of the system of electrons for chemical predictions.<sup>33</sup> DFT study, combined with experimental investigation, has been a powerful tool to predict the ORR mechanism. It also helps to screen and design electrocatalysts. In this regard, Keith *et al.*<sup>33</sup> depicted various possible ORR pathways on Pt (111) by DFT calculation. They investigated the binding energies for different possible intermediates in ORR: H, H<sub>2</sub>, O, O<sub>2</sub>, OH, OOH, H<sub>2</sub>O<sub>2</sub>, and H<sub>2</sub>O with consideration of multiple binding sites for various intermediates. Based on the calculated results of binding energies and bond strengths for free and adsorbed species on Pt (111), the possible pathways, shown in Fig. 2, can be constructed. Three pathways are distinguished: (a) the first is that, after oxygen adsorption, O<sub>2</sub>\* can firstly dissociate into 2O\*, which then react with hydrogen to form water; (b) alternatively, the second is O<sub>2</sub>\* reacts with hydrogen to firstly form OOH\*. OOH\* further dissociates into O\* and OH\*, which then react with hydrogen to form water; and (c) the third way is that OOH\* reacts with hydrogen once again to form H<sub>2</sub>O<sub>2</sub>\*. Then H<sub>2</sub>O<sub>2</sub>\* dissociates into 2OH\*, which finally react with hydrogen to form water. The key feature of the above pathways is when the O–O bond breaks.<sup>33</sup> For the initial stages of oxygen reduction at the Pt (111)/water interface as a function of potential, Janik *et al.*<sup>41</sup> suggested that the reduction of adsorbed molecular oxygen occurs through electron transfer prior to protonation, synchronously with proton diffusion toward the electrode, and subsequently with OOH\* formation. Based on the detailed *ab initio* simulation of thermodynamic and kinetic parameters on the Pt (111) surface, the oxygen dissociation and the hydroperoxyl dissociation pathway are found to determine the overall reaction kinetics and to result in the double Tafel slope on Pt

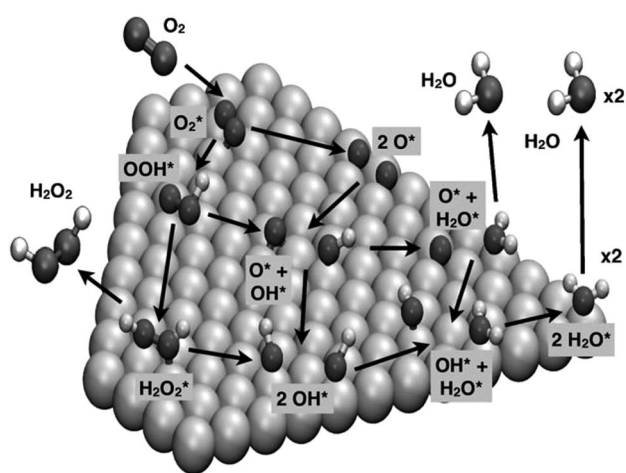


Fig. 2 Schematic representation of the various possible ORR pathways. Reprinted with permission from ref. 33. Copyright (2010) John Wiley and Sons.

(111).<sup>42</sup> In Fig. 2, the first and the second pathways follow the “direct” four-electron manner, and the third one is the “indirect” two-electron manner. Direct dissociation of O<sub>2</sub> has an activation barrier of >0.5 eV, rendering the first pathway an unlikely reaction step.<sup>43</sup> On the different active catalysts, the ORR follows different mechanisms. For example, two-electron reduction was reported for less active metals such as Au and Hg, and four-electron reduction is generally believed to occur for the most active catalyst Pt.<sup>26</sup> Katsounaros *et al.*<sup>44</sup> suggested that hydrogen peroxide electrochemistry on platinum can be used to understand the ORR mechanism, as the applied potential determines the Pt surface state, which is then decisive for the direction of the reaction: when H<sub>2</sub>O<sub>2</sub> interacts with reduced surface sites, it decomposes to adsorbed OH species; when it interacts with oxidized Pt sites, H<sub>2</sub>O<sub>2</sub> is then oxidized to O<sub>2</sub> by reducing the surface.

A combination of density functional theory with a modified Poisson–Boltzmann theory was used to calculate the formation of H, OH and O adsorbate on Pt (322) and Pt (111) by Nagoya *et al.*<sup>45</sup> It supports the experimental observation that the ORR activity increases on several stepped Pt surfaces because the OH adsorbates are destabilized with decreased solvation. ORRs on high-index planes of Pt *n*(111)–(111) were studied by Yue *et al.*<sup>37</sup> One of the two O atoms produced from the bond dissociation of O<sub>2</sub> pushes the other one down a step with lower binding energies, consequently reducing the energy required for the protonation reactions (O + H<sup>+</sup> → OH, and OH + H<sup>+</sup> → H<sub>2</sub>O). Although one O atom has strong binding on the edge of the Pt surface, the overall reaction benefits from the lower activation energy at the edge for O<sub>2</sub> bond dissociation, as well as weaker binding for O and OH sites as one of the O atoms moves down the step. These results suggest higher ORR activity on the high-indexed facets than on the low-indexed ones.

Unfortunately, no definitive conclusion on ORR kinetics has been made because of the dependence on environmental parameters such as concentration, solvent, thermodynamic energies, and the presence of an external electrode potential. The explicit description of the environment of the catalytic active site at the atomic scale is an ongoing challenge for theoretical approaches. Solvent effects were taken into account by applying continuum Poisson–Boltzmann theory to the bound adsorbates and to the transition states of the various reactions on the platinum (111) surface by Sha *et al.*<sup>46</sup> Morais *et al.*<sup>47</sup> attempted to model three effects of the environment: surface hydroxyl coverage, temperature, and reactant pressure. Liao *et al.*<sup>35</sup> monitored O<sub>2</sub> concentration near the Pt surface during ORR in 0.1 M HClO<sub>4</sub> using rotating ring-disk electrode (RRDE) system. They found that O<sub>2</sub> concentration near the Pt disk electrode surface changes sensitively with electrode rotation speed, applied electrode potential, and the rate and direction of the potential scan. At >0.8 V, O<sub>2</sub> concentration near the Pt electrode surface increases sensitively with the increasing potential. O<sub>ads</sub>|OH<sub>ads</sub> accumulates with ORR time. The accumulation rate increases with electrode rotation speed and potential. This confirmed that the reaction rate for O<sub>2</sub> + 2H<sup>+</sup> + 2e → 2OH<sub>ads</sub> is faster than that for the removal of OH<sub>ads</sub> to H<sub>2</sub>O under such conditions.<sup>35,48</sup> Based on their model study, Zhang

*et al.*<sup>49</sup> suggested that the rate of the four-electron reduction is a function of the rate constants for more than one electron transfer step, with no one step dominating.

## 2.2 Catalyst design

The Sabatier principle is a qualitative concept in catalysis, which states that the interaction between the catalyst and the substrate should be “just right”. That is, neither too strong nor too weak. ORR activity is controlled by oxygen binding to the surface, which should be not too weak (to split  $O_2$  molecules) and not too strong (to allow easy desorption of hydroxyl and water products). Pt has shown better ORR activity than other single-element catalysts such as Pd, Ir, Ag, Au, Co, Ni, Ru, and Cu, because of its appropriate electronic structure for oxygen- and OH-binding energies,<sup>6</sup> although its surface binds oxygen a little stronger than the optimal.<sup>50</sup>

Nørskov *et al.*<sup>6</sup> emphasized that the most optimal metal catalyst for ORR has an OH adsorption energy ( $\Delta E_{OH}$ ) of 0.1 eV, weaker than Pt (111). Pt alloying presents a way of adjusting the binding of the Pt surface. The sublayer Ni of  $Pt_3Ni$  alloy, the “most optimal ORR electrocatalyst” ever reported, imposes strong preferences in binding sites for most intermediates, which in turn strongly influence the reaction barriers.<sup>51</sup> Stephens *et al.*<sup>52</sup> also confirmed that the presence of subsurface 3d metals can weaken the binding of a Pt surface to  $OH^*$ . They concluded that only a slight weakening of  $\Delta E_{OH^*}$  by  $\sim 0.1$  eV, relative to Pt (111), will lead to optimal activity for ORR, resulting in an 8-fold improvement in the oxygen reduction activity. Stamenkovic *et al.*<sup>21</sup> noted that the better catalysts should counterbalance two opposing effects. One is the relatively strong adsorption energy of  $O_2$  and reaction intermediates ( $O^{-2}$ ,  $O_2^{-2}$ ,  $H_2O_2$  and so on). The another is a relatively low coverage by oxygenated species and specifically adsorbed anions, according to the results of ORR on the Pt, Pt-skeleton and Pt-skin surfaces of  $Pt_3M$  ( $M = Ni, Co, Fe, Ti, V$ ) in 0.1 M  $HClO_4$  at 333 K. This relationship exhibits a ‘volcano-type’ behaviour.

By DFT study, Shao *et al.*<sup>53</sup> demonstrated that the nanoparticle size dependent behaviour is associated with the oxygen binding energies on the different Pt sites accessible on cuboctahedral particles of various sizes. DFT calculations showed that the (111) facets contribute the high activity observed on the 2.2 nm Pt particle due to a proper oxygen binding energy. A much higher binding energy at edge sites and even the (111) facet on a smaller particle causes much lower oxygen reduction kinetics.

The high-index surfaces of Pt  $n(111)-(111)$  can enhance ORR activity. Yue *et al.*<sup>37</sup> found that the binding energy of  $O_2$ , O, and OH were the highest along the edge of the step. However, the mechanism and binding sites have shown to differ from the non-stepped surface due to the limited positions for certain atoms/molecules to adsorb on. The stronger binding of one of the O atoms will force the other O atom to shift to weaker binding sites during its protonation into OH. It hence reduces the energy required for ORR on the stepped surfaces. In comparison with the commercial Pt/C catalyst, the Pt concave cubes enclosed by high-index facets, including (510), (720), and

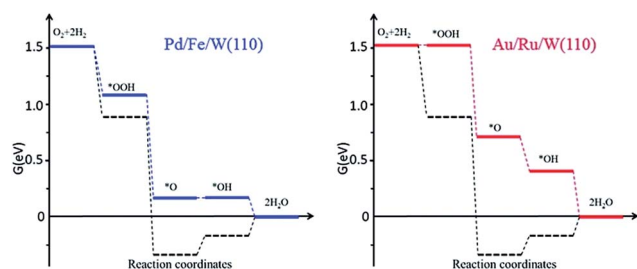


Fig. 3 ORR free-energy diagrams calculated for Pd/Fe/W (110) and Au/Ru/W (110) compared with that for Pt (111) (dashed black lines) for an electrode potential  $U = 0.85$  V. Reprinted with permission from ref. 55. Copyright (2012) American Chemical Society.

(830), exhibited a specific activity that is 3.6 times higher than the 3.2 nm Pt particles on Pt/C catalyst at 0.9 V.<sup>54</sup>

The “Design of Competitive Electrocatalysts” using theoretical and experimental knowledge now becomes possible. Stolbov and Ortigoza<sup>55</sup> designed tri-metallic sandwich-like structures of Pd/Fe/W (110) and Au/Ru/W (110). The constituting species are expected to couple synergistically, leading to high stability, cost-effectiveness, and tuneable reactivity. In Fig. 3, the free energy diagrams of the ORR reaction on Pd/Fe/W (110), Au/Ru/W (110) and Pt (111) were plotted at  $U = 0.85$  V, based on DFT calculations. All reaction steps on Pd/Fe/W (110) and Au/Ru/W (110) are shown to be exothermic, whereas the last two steps for Pt (111) are endothermic with significant thermodynamic barriers (0.15 to 0.2 eV). In other words, these diagrams indicate that the proposed materials are more active toward ORR than Pt (111). The success of this DFT study points to its potential in tailoring the reactivity of advanced materials.

## 3. Pt structure and morphology effects

ORR is structure-sensitive and heavily relies on the crystallographic orientation of the Pt surface.<sup>3</sup> Many efforts are devoted to structure control or morphology tailoring. Apart from 0-dimensional (0-D) Pt NPs, Pt morphologies with highly branched nanostructures (1-D) or thin film nanostructures (2-D) have attracted much attention.<sup>5</sup>

### 3.1 Structure and morphology

The electrocatalytic activity of an ORR catalyst depends not only on the ratio of the surface area to volume (morphology) but also on the structure or arrangement of atoms on the surface.

Platinum has a face-centered cubic (fcc) crystal structure. As illustrated in Fig. 4, the commonly observed Pt nanocrystals are all single crystalline in structure.<sup>56</sup> Pt (111), (100), and (110) index planes or facets are typically found on single-crystal surfaces of bulk Pt. Nanocrystals with a polyhedral shape are often enclosed by (111) and (100) facets. For example, Pt cuboctahedra have a mixture of (100) and (111) facets, while Pt cubes are enclosed by (100) facets. The tetrahedra, octahedra, decahedra and icosahedra are enclosed by (111) facets.<sup>54,57</sup>

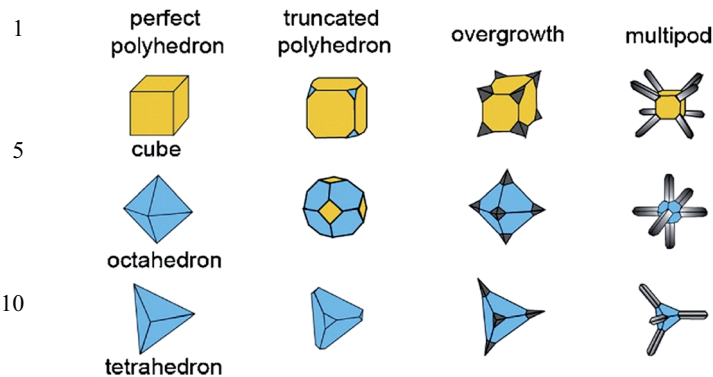


Fig. 4 Schematic illustration of different shapes of Pt nanocrystals derived from conventional single-crystal polyhedra enclosed by the low-index planes (100) and (111). The first column represents the perfect polyhedra; the second column contains the truncated forms of the perfect polyhedra; the third and fourth columns comprise the overgrown nanostructures and highly branched nanostructures grown from the corners of the perfect polyhedra, respectively. The yellow and blue colours represent the (100) and (111) facets, respectively. Reprinted with permission from ref. 56. Copyright (2009) Elsevier.

Commercial Pt/C catalysts are usually bounded by low-index facets such as (100) and (111).

The high index planes have high densities of atomic steps, edges, and kinks that act as active sites for breaking chemical bonds. The tetrahexahedral (THH) shape nanocrystal is bounded by 24 facets of high-index planes (730) and vicinal planes such as (210) and (310).<sup>57</sup> Concave nanocubes are mainly enclosed by (720) facets, together with some other high-index facets such as (510), (830), and (310).<sup>54</sup> As shown in Fig. 5,<sup>57</sup> the THH nanocrystals were imaged along the (001) direction, which was parallel to 8 of the 24 facets in the THH Pt nanocrystals. The selected-area electron diffraction (SAED) pattern in Fig. 5B revealed a 4-fold symmetry, which proved that the THH Pt nanocrystal was a single crystal. The high-resolution TEM image in Fig. 5C revealed a lattice spacing of 0.20 nm for the (200) planes of the THH Pt nanocrystal. The Miller indices of the exposed facets in Fig. 5A were calculated by measuring the angle between the facets. The values of  $133.6^\circ \pm 0.3^\circ$  and  $137.6^\circ \pm 0.3^\circ$  between the (730) facets are in good agreement with the theoretical values for  $\alpha = 133.6^\circ$  and  $\beta = 136.4^\circ$ . Therefore, the dominant facets of the THH Pt nanocrystals are (730) with contributions from (210), (310), and (520). This composition is evident in the atomic arrangement of the Pt (730) surface in Fig. 5D.<sup>57</sup>

Apart from 0-D Pt particles supported on carbon (Pt/C) catalysts, other shape platinum catalysts have been developed, such as 1-D Pt nanomaterials (Pt nanowires or Pt nanotubes), and 2-D thin films. As illustrated in Fig. 4, commonly observed Pt nanocrystals with a perfect single crystal structure, can be developed into truncated polyhedra (the second column), overgrown nanostructures from the corners (the third column) or facets (the fourth column).<sup>56</sup>

Preferred shapes or facets can be achieved by the controlled synthesis. In most cases, overgrowth is initiated from the corners or the facet of a polyhedral seed and further developed

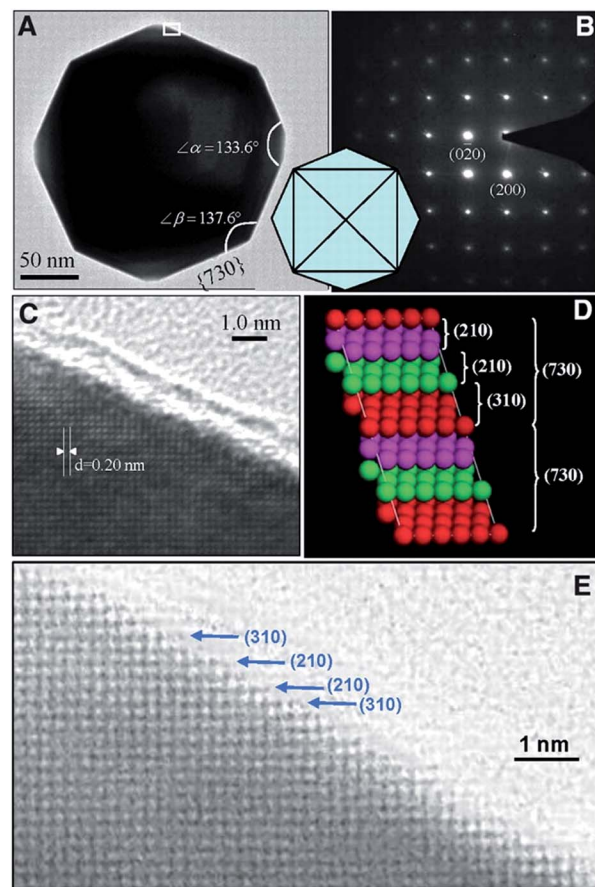


Fig. 5 Schematic illustration of tetrahexahedral (THH) nanocrystals with high-index planes. (A) TEM image of THH Pt nanocrystal recorded along the (001) direction. A careful measurement of the angles between the surfaces indicates that the profiles of the exposed surfaces are (730) planes ( $a = 133.6^\circ$ ,  $b = 136.4^\circ$ ). The inset is a (001) projected model of the THH. (B) Corresponding SAED pattern with square symmetry, showing the single-crystal structure of the THH Pt NC. (C) High-resolution TEM image recorded from the boxed area marked in (A). An amorphous thin layer is shown at the surface, which may be introduced by contamination during specimen handling and/or TEM observation. (D) Atomic model of the Pt (730) plane with a high density of stepped surface atoms. The (730) surface is made of (210) and (310) subfacets. The local surface of THH Pt NC can be (210) if the size of the crystal surface increases, although the overall profile of the facets is (730). (E) The image reveals the surface atomic steps. Reprinted with permission from ref. 57. Copyright (2007) The American Association for the Advancement of Science.

into a specified nanostructure. One-dimensional (1D) nanostructures with highly branched nanostructures, such as rods, wires, belts, and tubes, are characterized by a high aspect ratio.<sup>56</sup> Pt nanowires grow along the (111) axis,<sup>58</sup> and can be assembled into 3D flowerlike superstructures.<sup>59</sup> Pt nanowires grow perpendicular to the (111) crystallographic plane and the surface appears to consist of at least both (111) and (100) terraces.<sup>60</sup>

On the other hand, a two-dimensional (2D) nanostructured thin film (NSTF)<sup>61</sup> and a mesoporous double gyroid (DG) structured platinum,<sup>2</sup> both support-less, were investigated. They are much more stable than any supported nanoscale

1 catalyst. The metallic NSTF catalysts were prepared at 3 M by  
2 coating the desired metals on a perylene whisker substrate. This  
3 creates the so-called nanostructured thin film catalyst.<sup>61</sup> There  
4 is a distribution of surface atoms of approximately 61% (111)  
5 facets, 15% (100) facets, and 24% edge and corner sites. The  
6 atomic-scale model of the inverse DG structure reveals  
7 a different distribution of surface atoms to the commercial  
8 ETEK Pt/C catalyst, *i.e.*, 68% *vs.* 61% for (111) facets, 21% *vs.*  
9 15% for (100) facets, and 11% *vs.* 24% for edge and corner sites.<sup>2</sup>

### 3.2 Structure-controlled synthesis

10 Commercial Pt/C catalysts are often Pt nanocrystals with  
11 a polyhedral shape, which are enclosed by a mixture of (111)  
12 and (100) facets. Structure-controlled synthesis can be achieved  
13 in different conditions (such as solvent, Pt precursor, reducing  
14 agent and temperature, *etc.*) and processes.<sup>62–64</sup>

15 A wide range of physical and chemical methods has been  
16 developed to synthesize platinum NPs.<sup>62,65</sup> One can alter the  
17 surface energies with various capping agents, seeds, reductants  
18 and temperatures in a shape-controlled synthesis. Together  
19 with manipulation of the seed structures in the nucleation step  
20 by controlling the reaction kinetics and growing rate, different  
21 morphologies for the single crystal polyhedra can be achieved.<sup>56</sup>

22 The selectivity of a capping agent for a specific facet and its  
23 concentration play important roles in the formation of well-  
24 defined polyhedra.<sup>56</sup> Sodium polyacrylate (PAA) was used as  
25 a capping reagent by many authors for structure-controlled  
26 synthesis. Ahmadi *et al.*<sup>66</sup> developed a colloidal method for  
27 preparing Pt NPs with controlled shapes under assistance of  
28 sodium polyacrylate polymer as a capping reagent. Tetrahedra  
29 were synthesized with H<sub>2</sub> as a reducing agent in the presence of  
30 sodium polyacrylate. Inaba *et al.*<sup>67</sup> synthesised single cubic Pt  
31 NPs with Pt (100) faces from a solution of K<sub>2</sub>PtCl<sub>4</sub> in the pres-  
32 ence of sodium polyacrylate as a capping reagent. When the  
33 polymer of MW = 5100 was added at a molar ratio of Pt/PAA = 1/  
34 12, cubic platinum NPs of an average size of 10.3 nm were  
35 predominantly formed (*ca.* 50% in number) at 25 °C. The elec-  
36 tron diffraction of the particles revealed that they were single  
37 crystals with Pt (100) facets on the surface. After repeated  
38 potential cycling in the range 0.05–1.4 V, the features of Pt (100)  
39 were lost, and changed to those of polycrystalline Pt with Pt  
40 (110) and Pt (111).

41 Synthesis of the unconventional Pt nanocrystals covered by  
42 high-index facets is difficult because of their high surface  
43 energies.<sup>68,69</sup> Tetrahedral (THH) nanocrystals with high-  
44 index (730), (210), and/or (520) facets were prepared under  
45 a square wave potential (a pulse sequence that alternates  
46 between reducing and oxidizing potentials at a rate of 10 Hz),  
47 where surface capping by gaseous species may play a part in  
48 directing or controlling the shape of a nanocrystal.<sup>57</sup> Br<sup>-</sup> ion  
49 serves as a capping agent to block the growth of the (100) axis  
50 for the first synthesis of Pt concave nanocubes enclosed by high-  
51 index facets. The Pt concave nanocubes, which selectively  
52 overgrow from corners and edges, were prepared by slowly  
53 adding an aqueous NaBH<sub>4</sub> solution and a mixture containing  
54 K<sub>2</sub>PtCl<sub>4</sub>, KBr, and Na<sub>2</sub>H<sub>2</sub>P<sub>2</sub>O<sub>7</sub> into deionized water. The surface

1 of a Pt concave nanocube was mainly enclosed by (720) facets,  
2 together with some other high-index facets such as (510), (830),  
3 and (310).<sup>54</sup>

4 Meng *et al.*<sup>60</sup> investigated the template-free synthesis of Pt  
5 nanowires *via* the chemical reduction of Pt precursors with  
6 formic acid. HCOOH was used as not only a reducing agent but  
7 also a structure-directing agent (a capping agent). Over a broad  
8 pH range, the aspect ratio of the Pt nanowires was strongly pH  
9 dependent. The anisotropic growth of Pt along the (111) direc-  
10 tion occurred at pH values up to 3; when the pH ≥ 4.5, it was  
11 largely suppressed. Pt growth along the (111) direction is  
12 explained by HCOOH capping of other Pt faces. Many authors  
13 also reported a surfactant-free or template-free method with  
14 formic acid as a reducing agent to grow Pt nanowires on multi-  
15 walled nanotubes (MWCNTs),<sup>70</sup> carbon paper<sup>71,72</sup> and carbon  
16 black.<sup>73,74</sup> Bu *et al.* reported<sup>75</sup> an efficient synthetic strategy to  
17 prepare selectively highly controllable platinum nanocrystals  
18 with distinct dimensionalities from one dimensional nanowires  
19 to zero-dimensional octahedra. Yao *et al.*<sup>76</sup> firstly designed  
20 a porous carbon matrix and grew directly Pt nanowires in the  
21 pore walls, forming a so called “Pt nanowire electrode”. Based  
22 on this matrix structure, the Pt nanowire morphology and  
23 distribution in the cathode layer can be accurately adjusted by  
24 carbon materials and thickness of the matrix, preparation  
25 processes, ionomer contents and Pt loadings.<sup>77–81</sup>

26 The seed- or nuclei-mediated growths were also used in Pt  
27 nanoparticle control. Pt or Pt alloy NPs were pre-deposited onto  
28 a carbon support as nuclei, followed by Pt pulse electrodeposi-  
29 tion.<sup>82</sup> This new approach was able to overcome aggregation  
30 issue of Pt NPs and improve their catalytic performance. The  
31 technology can also be used for the preparation of core/shell Pt/  
32 C electrodes when non-Pt or Pt alloy NPs are used as seeding  
33 materials.<sup>82</sup> Carbon-supported Pt NPs with various loadings of  
34 Pt were also prepared. During a novel seed-mediated growth  
35 method using hydroquinone (HQ) assisted selective deposition,  
36 the Pt nanoparticle size increases linearly from 3 nm to about 5  
37 nm with a slightly elongated and irregular shape.<sup>83</sup> Compared to  
38 the commercial Pt/C (40 wt%, JM), the as-prepared Pt/C samples  
39 showed a slightly lower binding energy of Pt 4f<sub>7/2</sub>. In particular,  
40 the valence band spectra showed a linear shift of the d-band  
41 centre toward the Fermi level with increasing amount of Pt  
42 deposited.<sup>83</sup>

43 Thin film<sup>2,84</sup> and nanowire network structures<sup>85,86</sup> were  
44 successfully prepared. Fig. 6 shows the synthesis procedure for  
45 mesoporous DG platinum.<sup>2</sup> The DG structure was synthesized  
46 by electrodeposition of Pt into a mesoporous silica film that  
47 served as a template atop a glassy carbon (GC) disk. This  
48 structure has an average pore-to-pore distance of 6.7 nm and  
49 a pore diameter of 3–4 nm with a surface area of 56 m<sup>2</sup> g<sup>-1</sup> Pt.<sup>2</sup>  
50 Nanostructured thin film (NSTF) catalysts are formed by  
51 vacuum sputter-deposition of catalyst alloys onto a supported  
52 monolayer of highly oriented crystalline organic-pigment  
53 whiskers. The Pt whisker support has a high aspect ratio (20–50)  
54 with a 0.6–2 μm length, a rectangular lath-like morphology, a  
55 55 ± 12 nm width and a 27 ± 7 nm thickness.<sup>84</sup> The nanowire  
56 network structures with Pt NWs and highly dispersed Pt NPs  
57 can eliminate the need for a conducting support. A platinum

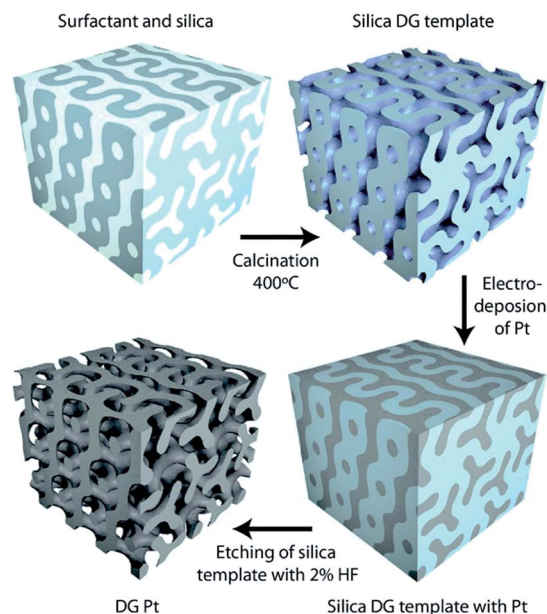


Fig. 6 Synthesis procedure and structural model for mesoporous DG platinum. Reprinted with permission from ref. 2. Copyright (2012) American Chemical Society.

nanowire network (approximately  $\varnothing 4$  nm) with silica nanoparticle (Pt net/SiO<sub>2</sub>) spacers was prepared *via* spray drying and hydrogen reduction. The platinum nanowire networks of the prepared catalysts showed branching and crossing of the nanowires. The average diameter of the platinum nanowires in Pt net/SiO<sub>2</sub> (4.5 nm) was less than that of the platinum nanowires in Pt net/C (5.2 nm).<sup>86</sup> Niu *et al.*<sup>87</sup> highlighted the importance of anisotropic growth and site-dependent phase segregation and migration mechanisms for controlling the compositional heterogeneity in bimetallic nanostructures, offering a radically different approach for the fabrication of nanocatalysts with enhanced performance.

### 3.3 Activity

The ORR activity is affected by Pt single-crystal surfaces. This dependence is attributed to the structure sensitive adsorption of intermediate species, such as O<sub>ads</sub> and OH<sub>ads</sub>.<sup>88</sup> Many studies showed that low-index planes or facets (111), (100), and (110), typically found on single-crystal surfaces of bulk Pt, have much lower activity than high-index planes. The high-index planes have high densities of atomic steps, ledges, and kinks that act as active sites for breaking chemical bonds.<sup>62</sup>

The anions in the electrolyte are believed to compete with the adsorption process and affect the overall ORR kinetics.<sup>89</sup> In perchloric acid solution, the kinetics are relatively insensitive to the crystal orientation. The Pt facet effect on the activity is in the order: Pt (110) > Pt (111) > Pt (100). Sulfuric acid has a strongly “interfering” nature as compared to the “non-interfering” nature of the perchloric acid electrolyte. Its kinetics are affected by the crystal orientation in electrolytes with the relative reactivity given by Pt (110) > Pt (100) > Pt (111).

In practical polymer fuel cell application, DuPont Nafion™ resin is generally used as ionomer and adhesive in the cathode. A study on well-defined Pt single crystals in the Nafion™ environment showed that the Pt (111) surface is more active than the Pt (100) surface for ORR. The difference in activity is more prominent for the high current density regime. This suggests that Nafion™ resin acts as a non-interfering electrolyte for electrochemical reactions, which also means that counter ions in the Nafion™ electrolyte do not affect the chemical kinetics.<sup>88</sup> Therefore, the Pt (111) facet is most desirable in Pt-based electrocatalysts for ORR in PEM fuel cell applications.

Decreasing the under-coordinated Pt atoms or surface defects is considered to contribute to activity enhancement. Under-coordinated Pt atoms, found on step sites, corner sites, and edge sites, *etc.*, are expected to be less active for the ORR than atoms on the flat planes because under-coordinated Pt atoms will form a much stronger bond to key reactive intermediates on the surface such as O<sub>ads</sub> and OH<sub>ads</sub>. The DG Pt structure exhibits a smaller fraction of under-coordinated surface sites compared to Pt/C, despite the fact that both possess similarly high surface areas.<sup>2</sup> It was found that the selective deposition of additional Pt takes place mainly on high surface energy Pt sites, *i.e.*, low coordinating Pt atoms, and increases the onset potential for OH adsorption.<sup>90</sup>

The one issue with the shape-controlled Pt NPs is their stability under ORR conditions as they tend to evolve into a thermodynamically equilibrated shape. For example, the non-crystal dendritic shape of the PtD/C disappeared due to the collapse of the structure after the potential cycling of the accelerated durability test (ADT).<sup>91</sup> In contrast, meso-structured platinum thin films with fewer under-coordinated Pt sites than Pt/C NPs showed enhanced activity and durability.<sup>2</sup>

## 4. Platinum size effects

A small Pt particle size has been preferred for a long time as the finely dispersed Pt on porous supports can maximize the electrochemically active surface area (ECSA, m<sup>2</sup> g<sup>-1</sup> Pt) and area-specific activity (j<sub>s</sub>, A m<sup>-2</sup> Pt). The mass activity (MA, A g<sup>-1</sup> Pt), the product of j<sub>s</sub> and ECSA, is the most important parameter for the ORR. As the size of a nanometal cluster further decreases to the sub-nanometre scale and ultimately to an atomic level (an atomically dispersed metal catalyst), the MA does not increase linearly, as the Pt particle size effect on the ORR is a complicated phenomenon, related to size distribution, shape, and inter-particle distance. In addition, the intrinsic stability of Pt electrocatalysts is also closely related to the size of Pt NPs, as smaller Pt NPs are more vulnerable to dissolution due to the decreased cohesive energy.<sup>3,28</sup>

### 4.1 Synthesis with controlled Pt sizes

It is known that the commercial Pt/C catalysts prepared by conventional methods usually showed a broad distribution of sizes (2–5 nm). Some novel processes for synthesis with controlled Pt sizes, such as the nanocapsule method,<sup>92</sup> modified

Pt UPD (underpotential-deposited)<sup>53</sup> and electron reduction,<sup>93</sup> were developed.

To obtain control of the particle size in a narrow range, Yano *et al.*<sup>92,94</sup> developed a modified nanocapsule method to prepare Pt and Pt-M (M = V, Cr, Fe, Co, and Ni) alloy NPs, highly dispersed on carbon black as ORR catalysts. Pt/C or Pt-M alloy/C were synthesised within nanocapsules formed in diphenyl ether in the presence of carbon black. The average Pt diameters on Pt/C ranged from 2.0 to 2.5 nm, regardless of the catalyst-loading level from 10 to 55 wt% on carbon black.<sup>92</sup> Recently, they used the above method to prepare Pt/C catalysts with average particle sizes of 2, 3, and 4 nm, each with a very narrow standard deviation (*ca.* 10%). The Pt particle size was controlled by changing the molar ratio of the metal precursor Pt(acac)<sub>2</sub> to surfactant in the solvent.<sup>94</sup> An exclusively modified microwave-assisted polyol method was developed for synthesis of carbon supported Pt and PtCr nanomaterials.<sup>95</sup> Diethylene glycol was used as both a solvent and reducing agent. The pH value at which the metal precursors are dissolved is the critical parameter to control the nanoparticle formation.

An *in situ* reductant strategy was suggested to control Pt particle growth in these syntheses.<sup>96</sup> This strategy involves, firstly, a gradual and homogeneous formation of hydroxide ion by hydrolysis of urea at an elevated temperature to form a homogeneous deposition of Pt-hydroxide complex species on the carbon support. Then,  $\gamma$ -ray radiolysis was applied to the deposited Pt-hydroxide complexes to produce homogeneously dispersed and ultra-small (2.2–3.1 nm) metallic Pt NPs on carbon support.

Shao *et al.*<sup>53</sup> used a Cu\_UPD\_Pt replacement method to prepare different Pt particle sizes by layer deposition. Pt NPs with an average particle size of 1.3 nm supported on Ketjen Black (specially synthesized by Tanaka Kikinokogyo (TKK), 10 wt%) were used as seeds for particle growth. After depositing 2, 4, and 10 layers of Pt, NPs with average sizes of 1.84, 2.46, and 4.65 nm are manufactured, respectively. All the samples have small standard deviations in the range of 0.2–0.3 nm indicating that the high mono-dispersity in particle size was maintained during particle growth. The Pt particles at the sub-nanometre scale are highly unstable and prone to agglomeration due to their high surface energy. The carbon supports show inert characteristics and do not provide strong metal-support interactions to stabilize the smaller Pt (less than 1 nm) particles.

Recently an atomically dispersed Pt catalyst was selectively synthesized *via* a simple wet-impregnation method on zeolite-templated carbon (ZTC) containing an extra-large amount (up to 17 wt%) of sulfur.<sup>30</sup> The S-doped ZTCs were synthesized by chemical vapour deposition of acetylene/H<sub>2</sub>S in NaX zeolite at 823 K. Subsequently, the samples were heat-treated at 1073 K under a H<sub>2</sub>S/He atmosphere. After etching with an HCl/HF (1.1/0.8 wt%) aqueous solution to remove the zeolite template, Pt was supported on the prepared carbons by a conventional wet-impregnation method. Bright-field transmission electron microscopy (TEM) images (Fig. 7a–c) show that Pt clusters having *ca.* 4 nm diameter were dispersed in Pt/ZTC (Fig. 7a), while 1–2 nm Pt clusters were present in Pt/LSC (low sulfur content; with a 4 wt% content of sulfur) (Fig. 7b). In Pt/HSC

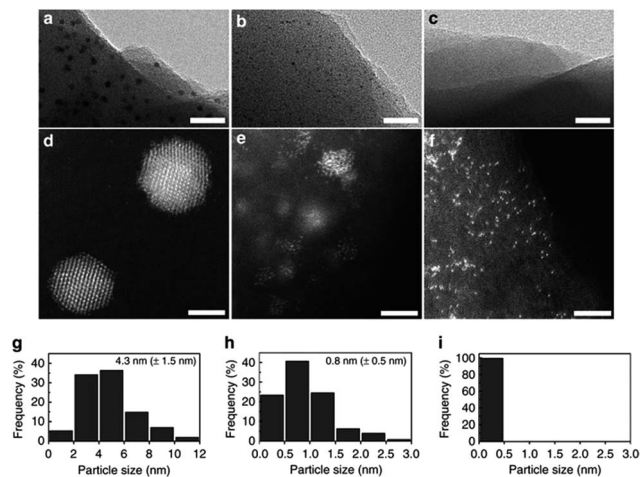


Fig. 7 Structures of atomically dispersed Pt species on the catalysts. (a–c) TEM images indicating the presence of *ca.* 4 nm Pt clusters in Pt/ZTC (a), Pt clusters (1–2 nm) in Pt/LSC (b), and the absence of discernable Pt species in Pt/HSC (c); scale bar, 30 nm. (d–f) To visualize the dispersion and structure of sub-nanometre Pt species, atomic resolution HAADF-STEM images are additionally provided for Pt/ZTC (d), Pt/LSC (e), and Pt/HSC (f); scale bar, 2 nm. (g–i) Histograms of the particle size distributions for Pt/ZTC (g), Pt/LSC (h), and Pt/HSC (i). The images reveal that Pt/LSC contains both atomically dispersed Pt species and Pt clusters. Pt/HSC contains mainly the atomically dispersed Pt species. Reprinted from ref. 30. Copyright © 2016, rights managed by Nature Publishing Group under a Creative Commons CC-BY license.

(high sulfur content; with a 17 wt% content of sulfur) (Fig. 7c), no Pt cluster was discernible in TEM. To visualize further sub-nanometre Pt species, atomic resolution high-angle annular dark-field scanning transmission electron microscopy (HAADF-STEM) was conducted (Fig. 7d–f) along with particle size distribution analysis (Fig. 7g–i). On the Pt/HSC (Fig. 7f), Pt exists mainly as an atomically dispersed species without appreciable Pt clustering. They conclude that abundant S-functionalities and the unique carbon structure (that is, highly curved three dimensional networks of graphene nanoribbons) contribute to stabilize a relatively high loading of Pt (5 wt%) in the form of atomically dispersed Pt.

#### 4.2 Pt size effects on activity and stability

The Pt particle size effect on ORR activity has been a long-standing problem that has yet to be solved. The main reason for the discrepancy may result from the fact that the activities of Pt were measured in different types of electrolyte and on different samples that may have different shapes and degree of agglomeration.<sup>5</sup> In addition, because of a lack of image and probe techniques to identify directly the arrangement of the surface atoms of a Pt particle and broad size profiles, the Pt facet effect cannot be involved.

Pt alloys with two compositions demonstrated that the relationship of size–ORR activity relies on the surface.<sup>97</sup> The octahedral Pt<sub>3</sub>Ni/C exhibited a steady increase in the ORR activity with particle size in the range 4.5–8.1 nm, due to the significant size-variation of ORR activity, which was attributed

to the size dependent change in the fraction of (111) terraces. In comparison, the octahedral Pt<sub>1.5</sub>Ni/C exhibited a different size dependency on ORR activity, a volcano relationship between the ORR activity and the Pt<sub>1.5</sub>Ni size, which could be caused by the interplay between lower stability and a higher fraction of (111) terraces of the larger octahedral Pt<sub>1.5</sub>Ni particles. They explained the maximal mass activity at 2.2 nm based on density functional theory calculations performed on fully relaxed NPs.<sup>97</sup> Li *et al.*<sup>98</sup> found that the ORR activity of well dispersed and uniform Pt NPs is indeed dependant on their size, and the effect is decreased in the range 2–7 nm.

In the range of 1–5 nm, Shao *et al.*<sup>53</sup> examined the relationship between the Pt particle size and oxygen reduction activity in HClO<sub>4</sub> solution. Their results clearly show that both mass and specific activities depend on the Pt particle size. In Fig. 8, the relationship of size dependence of specific activity (blue diamond) and mass activity (red square) of Pt/C is shown for ORR at 0.93 V.<sup>53</sup> The area specific activity increases rapidly by 4-fold as the particle size grows from 1.3 to 2.2 nm and increases slowly as the particle size further increases. On the other hand, a maximum Pt mass activity was observed at 2.2 nm. They also estimated an average particle size of 2.5 nm for the state-of-the-art Pt/C catalyst with an almost maximum mass activity, very near to the optimal size of 2.2 nm.<sup>53</sup>

Another investigation<sup>99</sup> revealed a size-independent ORR activity of Pt NPs below 5 nm, which was attributed to the similar surface compositions and surface electronic structures of Pt NPs below 5 nm as well as comparable OH anion coverage at the potential where ORR was evaluated. In contrast, the instability of Pt NPs under accelerated potential cycling was found to be strongly dependent on the particle size. This group thought that the TEM-measured “particle size” was not accurate

to describe the ORR behaviour of different sized Pt NPs obtained from TKK due to the TEM detection limit on extremely small particles (<0.5 nm). It is therefore suggested that ESA should be used to describe the so-called “size effect” on NPs as it better reflects the particle size and size distribution.

Size effects of Pt NPs on the ORR mechanism were also reported. Inaba *et al.*<sup>100</sup> found a size effect of Pt NPs ascribed to peroxide formation. It was recently found that atomically dispersed Pt significantly differs from cluster-type Pt catalysts in terms of electro-chemical behaviour: the former selectively catalyses a two-electron ORR pathway producing H<sub>2</sub>O<sub>2</sub>, rather than the conventional four electron ORR pathway producing H<sub>2</sub>O.<sup>30</sup>

Pt nanoparticle stability must be taken into consideration as the degradation of Pt NPs in fuel cell cathodes leads to the loss of the precious metal catalyst. Under a fuel cell environment, Pt particles suffer from Ostwald ripening and agglomeration (so-called sintering or coalescence). For Ostwald ripening, Pt particle size increases *via* a dissolution–redeposition process as a result of redox cycling, whereas, for agglomeration, small particles merge into big particles. These processes will lead to a decrease of the ECSA and to activity degradation.

Contrary to the common view, Yano *et al.*<sup>94</sup> found that Pt NPs as small as 2 nm were quite durable among 2, 3 and 4 nm home-made Pt/C catalysts and commercial 2 nm Pt/C. They thought that NPs, being uniform in size and highly dispersed over the whole surface of the carbon support, are the key to catalyst durability.

Ostwald ripening and agglomeration are difficult to distinguish in experiments. Escaño<sup>101</sup> conducted first-principles calculations based on density functional theory to determine effect of the smaller particle (1–2 nm) shapes on Pt dissolution and coalescence. For dissolution, the stability of the Pt NPs increases in the following order: hexagonal close-packed < icosahedral < cuboctahedral < truncated octahedral. This trend is attributed to the synergy of the oxygen adsorption strength and the local coordination of the Pt atoms. The stability of the Pt NPs was found to increase in the following order: hexagonal close-packed < truncated octahedral < cuboctahedral < icosahedral. This correlated with the cohesive energies of the particles. The new “metal-interfaced” Pt-based core–shell architectures should be more stable than pure Pt NPs with respect to both dissolution and coalescence.<sup>101</sup> Shi *et al.*<sup>102</sup> employed a combination of empirical potential simulations and DFT calculations to investigate the structure–function relationships of small PtN ( $N = 2–80$ ) clusters on model carbon (graphene) supports. Point defects in graphene anchor Pt clusters strongly and also affect appreciably the morphologies of small clusters. A key finding from the structural analysis was that the fraction of potentially active surface sites in supported clusters was maximized for stable Pt clusters in the size range of 20–30 atoms.

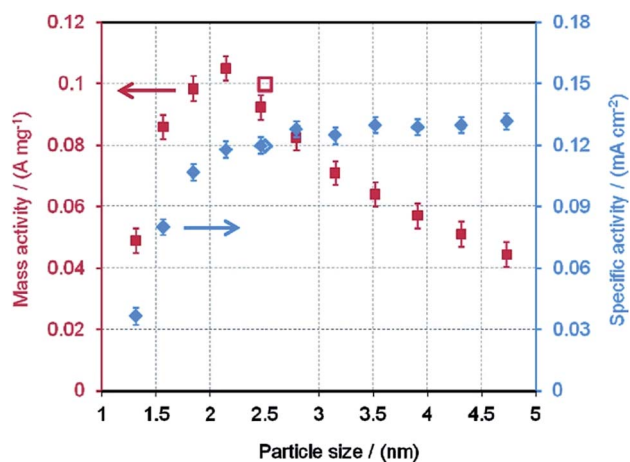


Fig. 8 Size dependence of the specific activity (blue diamond) and mass activity (red square) of Pt/C for ORR at 0.93 V. The specific activity (open blue diamond) and mass activity (open red square) of state-of-the-art Pt/C from TKK (TEC10E50E, 46.7 wt%) with an average particle size of 2.5 nm is also included for comparison. The specific and mass activities were calculated by normalizing the kinetic current to the electrochemical active surface and the Pt weight on the electrode, respectively. The Pt weight was calculated by the Cu UPD charge. Reprinted with permission from ref. 53. Copyright (2011) American Chemical Society.

## 5. Carbon supports and their stability

In order to maximize the surface area, Pt is typically deposited as NPs (2–5 nm) on a carbon support. Carbon materials possesses a high surface area, excellent electronic conductivity,

and chemical stability.<sup>6,103</sup> The development of highly dispersed metal NPs on carbon blacks brought considerable progress in fuel cell technology.<sup>104</sup> However, the carbon support could not present a strong affinity towards catalyst particles on which a uniform dispersion of Pt NPs can be achieved. The particle proximity effect was found by the observed weakening of the OH adsorption strength. This inhibits a distinction between the particle size and the particle proximity effect.<sup>65</sup> Carbon also suffers from corrosion, especially under some conditions such as start-up and fuel starvation in fuel cell operation.<sup>105</sup> Carbon corrosion may result in detachment of Pt NPs from the support. The Pt particles subsequently agglomerate into large particles or collapse into caves,<sup>28</sup> and hence affect the long-term stability of the Pt catalyst. Surface functionalization and graphitization of carbon blacks, carbon nanotube, graphene and promoted additives were introduced to improve ORR catalysts.

### 5.1 Carbon black

Carbon blacks have been widely used as support materials for fuel cell catalysts, because of their high electronic conductivities and surface areas.<sup>11</sup> The pore volumes of carbon blacks consisted primarily of pores smaller than 8 nm.<sup>106</sup> The interior surface area in carbon support particles is less favourable due to their inferior character in terms of mass transport for the electrode reactions.<sup>107</sup> A novel combination of mercury porosimetry with computerized X-ray tomography was suggested by Malik *et al.*<sup>108</sup> to probe the nanostructure of the catalyst layer. This method showed that a spatial arrangement of high-density regions created when using a screen-printing process has a relatively more accessible porosity.<sup>108</sup> Improvement of PEFC performance can be achieved by an optimal carbon support with a smaller pore volume (<8 nm) on the surface of the carbon primary particles so as to decrease the Pt absorbed in the small pores.<sup>106</sup> Park *et al.*<sup>107</sup> recently examined several carbon materials, carbon black (CB, 875 m<sup>2</sup> g<sup>-1</sup>), graphitized carbon black (GCB, 164 m<sup>2</sup> g<sup>-1</sup>) and acetylene black (AB-800 and AB-250, 779 m<sup>2</sup> g<sup>-1</sup> and 219 m<sup>2</sup> g<sup>-1</sup>) as Pt catalyst supports. The effective Pt surface area (S(e) Pt) increased in the following order: c-Pt/CB < c-Pt/GCB < n-Pt/AB800 < n-Pt/AB250. They ascribed the trend to the decreased hollow structures inside the carbon, since only the accessible electrocatalytic surface area can contribute to the ORR.

The active functional groups (*e.g.*, CO, COOH, and CN) on the surface of the carbon powder interact with metal precursors in the catalyst synthesis. Therefore they play a crucial role in the obtained nanoparticle size and dispersion.<sup>11,65</sup> Many researches showed the weak interaction could not support small metal particles (<1 nm). The nitrogen-doped carbons are considered to serve as anchoring sites for metal nanoparticle deposition, concurrently promoting catalytic reactions. A 1 nm-thick layer of pyridinic-N (N-doped carbon) on Pt/C catalyst enhanced the ORR activity and durability of the PEMFCs.<sup>109</sup> As the reduction rate of the pyridinic N was proportional to the degradation rate of the cell performances, it was deduced that the ORR activity may be strongly related to the pyridinic N in the NC layers.<sup>109</sup>

Wang *et al.*<sup>93</sup> recently reported a room temperature electron reduction method for the synthesis of a highly active and stable

carbon supported Pt (111) catalyst (Pt (111)-P/C) under peptide assistance. Such a prepared catalyst shows surface sites featuring predominately (111) facets with a small particle size around 2 nm. In comparison with commercial Pt/C catalyst prepared by conventional methods, the mass activity and specific activity of the Pt (111)-P/C catalyst for ORR are shown to increase by a factor of ~2. A 10 000-cycle durability test also showed a significantly enhanced stability over the commercial Pt/C catalyst.

Jung *et al.*<sup>110</sup> functionalized carbon supports for Pt (Pt/C) catalysts with thermally hydrophilic-hydrophobic responsive poly(*N*-isopropylacrylamide) (PNIPAM). Amine-terminated PNIPAM selectively reacted with the functional group of -COOH on the carbon surfaces of Pt/C *via* the amide reaction with 1-ethyl-3-(3-dimethylaminopropyl) carbodiimide. The PNIPAM-functionalized Pt/C was hydrophilic at room temperature during catalyst ink preparation, while at an operating temperature of 70 °C it was hydrophobic.

Carbon supports decorated by metal oxide have been studied by many authors. It was found that metal oxides can interact intensely with Pt particles.<sup>111</sup> Pt-Ta<sub>2</sub>O<sub>5</sub>/VC (Vulcan Carbon) catalyst was synthesized by deposition of tantalum oxide on VC, followed by the deposition of platinum colloids.<sup>112</sup> It was found that the area-specific activity of Pt-Ta<sub>2</sub>O<sub>5</sub>/VC for the ORR at 0.9 V was 1.5–2 times higher than that of standard Pt/VC. According to the d-band approach explored with density functional theory, tantalum(v) should bring down the d-band centre of platinum, which would result in a weaker bonding between platinum and adsorbed oxygen species. The higher area-specific activity of the catalyst may be due to the preferential adsorption of OH groups to the oxide *vs.* platinum surface.<sup>112</sup> CeO<sub>x</sub> was also introduced to improve Pt/C catalysts. A Pt-CeO<sub>x</sub>/C catalyst was prepared by a combined process of precipitation and co-impregnation methods, as schematically illustrated in Fig. 9.<sup>113</sup> Pt oxide formation was suppressed by the presence of CeO<sub>x</sub>, as Ce<sup>3+</sup> was oxidized to Ce<sup>4+</sup> instead of Pt at the Pt oxide formation potential. The inhibition of Pt oxide formation is considered to be the primary factor for enhancement of the ORR rate because the ORR activity of the Pt oxide surface is much lower than that at the bare Pt surface.

### 5.2 Carbon nanotubes (CNTs) and multi-walled nanotubes (MWNTs)

Carbon nanotubes (CNTs) are allotropes of carbon with a cylindrical nanostructure, generally categorized into single-walled nanotubes (SWNTs) and multi-walled nanotubes (MWNTs). MWNTs consist of multiple rolled layers (concentric tubes) of graphene. Carbon nanotubes have attracted interest due to their better conductivities, corrosion resistance, and mechanical/electrochemical properties compared with commonly used carbon blacks. CNTs have fewer impurities compared with commercial carbon blacks, while the sulphur impurities can poison the Pt electrocatalysts.

However, the smooth surface and chemical inertness of pristine CNTs could not bind or anchor metal NPs. CNTs are usually treated by harsh acid oxidation and functionalization.

Xiao *et al.*<sup>114</sup> reported a Mn<sub>3</sub>O<sub>4</sub> coated carbon nanotube for an oxygen reduction Pt electrocatalyst. They synthesized Mn<sub>3</sub>O<sub>4</sub>

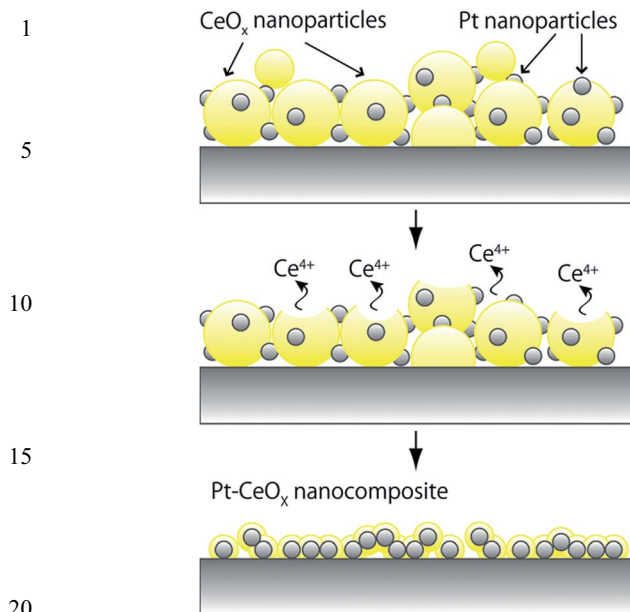


Fig. 9 Schematic illustration of structural change of the Pt–CeO<sub>x</sub>/C catalyst during pretreatment. Reprinted with permission from ref. 113. Copyright (2012) American Chemical Society.

nanoparticle coated carbon nanotubes (Mn<sub>3</sub>O<sub>4</sub>/CNTs) and self-deposited well-dispersed Pt nanocrystals on Mn<sub>3</sub>O<sub>4</sub>/CNTs to obtain Pt/Mn<sub>3</sub>O<sub>4</sub>/CNTs hybrid catalysts *via in situ* reduction of the support matrix. The self-deposited Pt could be ascribed to the galvanic replacement reaction between PtCl<sub>4</sub><sup>2-</sup> and Mn<sub>3</sub>O<sub>4</sub> with no need for any capping agent and additional reducing agent. Fig. 10a clearly shows that there are plenty of Pt nanocrystals (bright spots) with sizes around 2 nm uniformly decorated on the surface of the CNT composite with no obvious aggregation. Fig. 10c–f reveals elemental mapping distribution of C, O, Mn, and Pt elements in the composite. As a result of the good dispersion of Pt nanocrystals, the interconnected CNT conductive network, and a possible synergistic co-catalytic effect from heterojunction interfaces of Pt nanocrystals and Mn<sub>3</sub>O<sub>4</sub>, the as-prepared Pt/Mn<sub>3</sub>O<sub>4</sub>/CNTs hybrid catalysts demonstrated highly enhanced electrocatalytic activity for ORR.<sup>114</sup>

Du *et al.*<sup>115</sup> used commercially available nickel-coated GCs for the growth of single-crystal Pt NPs. PtNi–MWCNT hybrids possessed a high mass activity of 0.51 A mg Pt<sup>-1</sup>, nearly double that of TKK's state-of-the-art Pt/C catalyst. After an accelerated durability test by 2500 potential sweeping cycles, PtNi–MWCNTs still retained 89.6% of their initial mass activity, which is 0.46 A mg Pt<sup>-1</sup> and 4% higher than the DOE target of 0.44 A mg Pt<sup>-1</sup> for 2017–2020.

The phosphorus-doped carbon nanotubes (P-CNTs) supported Pt catalyst exhibits significantly enhanced electrocatalytic ORR activity and long-term stability due to the stronger interaction between Pt and P-CNTs, which is proven by X-ray photoelectron spectroscopic analysis and DFT calculations.<sup>116</sup> In contrast to the previously reported studies, Gupta *et al.*<sup>117</sup> found that the exceptionally high performance of Pt supported on defect-free, highly purified CNTs was achieved comparing

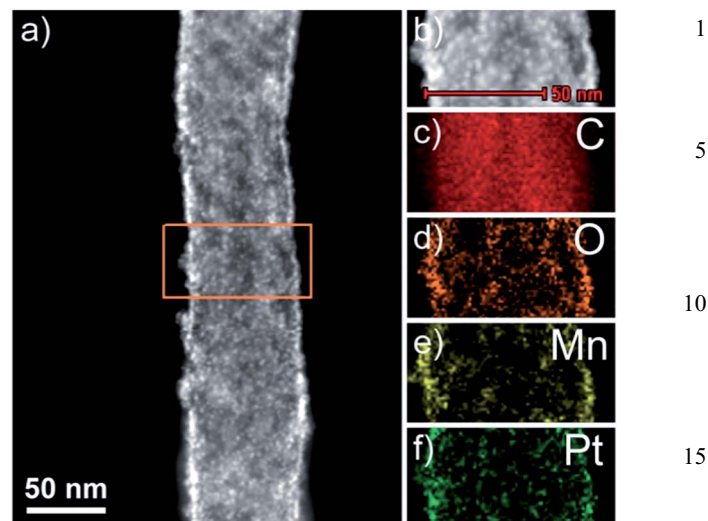


Fig. 10 (a and b) HAADF-STEM image of Pt/Mn<sub>3</sub>O<sub>4</sub>/CNTs. (c–f) Elemental mapping of the selected part shown in (b). Reproduced with permission from ref. 114. Copyright (2013). The Royal Society of Chemistry.

that on pristine CNTs. They attribute this to a neutral coordinate complex, which not only stabilizes the Pt NP, but also reduces the chances of its agglomeration.

### 5.3 Graphene

Graphene is another allotrope of carbon, in the form of a two-dimensional sheet of carbon atoms chemically bonded in the hexagonal pattern that is characteristic of graphite. Graphene has the ability to meet all criteria of ideal supports of platinum catalyst, including high surface area, electronic conductivity, electrochemical stability and the ability to distribute homogeneously uniformly sized NPs.<sup>118</sup> As graphene is a two-dimensional planar sheet with an open structure, there is the possibility of both sides of graphene and their tuneable surface being utilized for supporting catalysts.<sup>119</sup>

Graphene and its derivatives have emerged as promising platinum electrocatalyst supports.<sup>118,120</sup> Several main issues must be resolved before graphene can be used as a catalyst support: (a) the severe aggregation of Pt NPs on graphene surfaces; (b) the restacking of graphene layers due to van der Waals forces; (c) the poor dispersion of graphene in solvent; and (d) the strong tendency of graphene to agglomerate in aqueous solutions. These issues hinder graphene from reaching its full potential as a catalyst support for fuel cell applications. To improve its surface property and solubility, graphene can be modified through two common routes:<sup>120</sup> (a) doping with a single element (N, S, P and B) or bi-element doping (N and S, or N and B); and (b) chemical functionalization, like metal-oxide functionalized graphene, metal phthalocyanine functionalized graphene, sulfonated graphene and polymer/graphene.

The graphene-based supports, doped with heteroatom species, are distinct from functionalized graphene, as the foreign heteroatoms are incorporated directly into the graphitic planes.<sup>118</sup> A DFT study shows that enhanced platinum

adsorption in defective N-doped graphene can be mainly attributed to a strong hybridization between platinum orbitals and  $sp^2$  dangling bonds at the defect sites.<sup>121</sup> In contrast to doping, chemical functionalization using either covalent or noncovalent methods does not introduce impurities that could destroy the carbon network of graphene.<sup>120</sup>

Graphene oxide (GO), single or few layer graphene made from graphite oxide, has a high concentration of surface functional species and disperses in a large number of solvents.<sup>122</sup> Two different methods under moderate condition, namely the solar and hydrogen exfoliation of graphite oxide, for the large scale synthesis of high quality graphene sheets were developed by Vinayan *et al.*<sup>119</sup> Graphite oxide is the starting material prepared from purified natural graphite using Hummers' method.<sup>123</sup> The surface functional groups on the surface of graphite oxide facilitate its dissolution in different solvents. It is noteworthy that the number density of the functional groups can be varied on the surface by changing the extent of oxidation. It has also been suggested that these functional groups can serve as the anchors or nucleating centres for the controlled growth of NPs.<sup>119</sup> Xin *et al.*<sup>124</sup> developed a facile strategy to covalently graft *p*-phenyl  $SO_3H$  or *p*-phenyl  $NH_2$  groups onto the graphene surface. The functional groups were found to not only facilitate the homogeneous distribution of Pt NPs on the surface of graphene supports and reduce the Pt average particle size but also strengthen the interaction of the Pt atoms with the functional groups and, consequently, minimize the migration/coalescence of the Pt NPs in the course of accelerated durability tests.

Sulphur commonly causes issues due to Pt surface poisoning or contamination. Wang *et al.*<sup>125</sup> speculated that if sulphur could be immobilized within the graphitic framework of a support material, the strong interactions with it could be exploited in a favourable catalyst-support combination. To prepare sulphur doped graphene (SG), phenyl disulphide and GO were mixed together and heated in a furnace at 1000 °C for 30 min under the protection of high purity argon. The strong Pt-S interaction is essential to contribute to the uniform nucleation of Pt on SG, whereas non-uniform nucleation was observed on pristine graphene supports. Using SG as a support material, where the heterogeneous dopant atoms could serve as nucleation sites, SG supported Pt nanowire arrays were manufactured with diameters of 2–5 nm and dense surface coverage. They revealed that the structure of the resulting composite could be readily controlled by fine tuning the Pt nanowire nucleation and growth reaction kinetics in addition to the Pt-support interactions.<sup>118,125</sup> Electrochemical characterization shows that the SG composite materials have 2–3 times higher catalytic activities toward ORR compared with the commercial Pt/C catalyst.<sup>125</sup>

#### 5.4 Stability and durability

It is well known that the carbon support corrosion (thermodynamic potential 0.21 V), especially at high positive potentials, created during the fuel cell start-up/shutdown procedure, is a big problem and a significant challenge to be resolved in

future investigations. Here we only focus on some interesting concepts based on carbon materials that reduce or overcome carbon corrosion.

The results from Kim *et al.*<sup>126</sup> indicate that oxygen functionalization of Pt/C catalysts can have a positive impact on the initial activity for the ORR, but can exert an adverse effect on its long-term durability. Graphical illustrations of Pt dissolution processes over Pt/C catalysts are shown in Fig. 11. For oxygen-functionalized carbon support (CB\_O), the electrons in Pt NPs nearby oxygen groups could be withdrawn by highly electronegative oxygen. As a result, Pt NPs could be oxidized, the Oswald ripening takes place easily, and finally the ripening of Pt NPs was accelerated.

Graphitic carbon exhibits a higher resistance to carbon corrosion compared with non-graphitic carbon. Studies on catalytic electrodes with X-ray diffraction, Raman spectroscopy and transmission electron microscopy show that the graphitic carbon-support resists carbon corrosion and helps mitigate aggregation of Pt and  $Pt_3Co$  catalyst particles.<sup>127</sup> Kim *et al.*<sup>128</sup> synthesized a nitrogen-doped onion-like carbon with a nitrogen of 1.7 at% with a defective graphitic outermost shell, in which the edge and defective sites induced from nitrogen atoms effectively facilitated the nucleation of Pt clusters, leading to the stable dispersion and small size of Pt NPs. The less defective and intact inner shells of the nitrogen-doped onion-like carbon structure were responsible for improved durability due to their corrosion resistance. The graphitized 3D interconnected mesoporous network offered not only a high degree of graphitization, but also a high specific surface area and stabilization by Pt confinement to the pores, which results in a highly active and stable catalyst.<sup>129</sup> Similarly, a hollow carbon nanocage was developed with a high degree of graphitization and concurrent

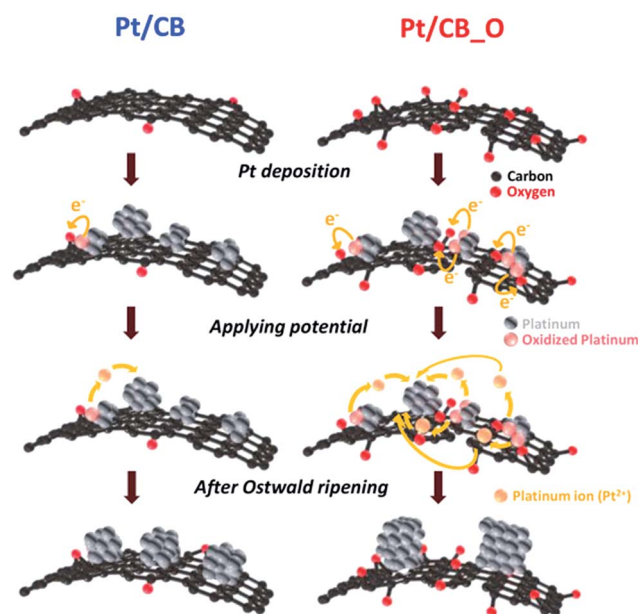


Fig. 11 Schematic illustrations of changes in Pt particle size distribution before and after the ADTs in Pt/CB and Pt/CB\_O catalysts. Reproduced with permission from ref. 126. Copyright © 2016 Elsevier Ltd.

nitrogen doping for oxidation resistance enhancement, uniform deposition of fine Pt particles, and strong Pt-support interaction.<sup>130</sup> Testing under conditions of practical fuel cell operation reveals almost no degradation over long-term cycling. Coating can also protect carbon from corrosion. Berber *et al.*<sup>131</sup> described the design and fabrication of a highly durable fuel cell electrocatalyst based on double-polymer-coated carbon nanotubes. A remarkable durability of 500 000 accelerated potential cycles was recorded with only a 5% loss of the initial fuel cell potential and 20% loss of the maximum power density. The unexpected high durability was achieved with an ionic liquid thin layer that exists between the Pt NPs and carbon support due to the suppression of carbon corrosion.<sup>132</sup> A sacrificial precursor based on a metal-organic framework was suggested by Lou *et al.*<sup>133</sup> Accelerating durability tests, after 16 000 potential cycles, demonstrated the higher stability of Pt/CeO<sub>x</sub>/C in contrast to the oxide-free and Pt/C (JM) catalysts. Li *et al.*<sup>134</sup> proposed a reversible preferential oxidation method to protect carbon carriers against oxidation. When the fuel cell operates at high potential, VO<sub>2</sub><sup>+</sup> is oxidized to VO<sup>2+</sup>. This preferential oxidation protects carbon carriers against oxidation. When the fuel cell returns to normal working potential, the VO<sup>2+</sup> is restored to VO<sub>2</sub><sup>+</sup>. VO<sup>2+</sup> is a reserve for the protection of carbon carriers at subsequent instances of high potential.

## 6. Conclusion and perspective

Significant progresses have been made recently in the study of Pt-based ORR catalysts over various carbon supporting materials. The major objectives of these studies are: (1) to design and prepare highly active Pt catalysts with low Pt content and excellent durability; (2) to obtain a full understanding of the Pt ORR catalyst. From the results reported, the following conclusions can be made: (1) the size of the Pt NPs has a significant effect. Based on the catalyst components, supporting materials and reaction conditions, an optimal catalyst size exists. However, the size effect is obviously a complicated issue for the supported Pt catalysts because of the complex reaction mechanism of ORR and the complicated structure-influencing factors. The present studies conducted for the size effects did not maintain the same catalyst structure with the same defect status because of the difficulty in the structure and defect control of the supported Pt catalysts. A small difference in the catalyst structure may cause a large error in comparative studies of the size effect. Therefore, there are still too many issues to be investigated for the size effect. (2) The catalyst structure has a great effect on the ORR activity. Higher ORR activities on high-index facets have been observed compared with those on the low-index ones. The challenges are how to fabricate the catalyst with such high-index facets and how to stabilize them. (3) The controlled synthesis of Pt NPs with both control of the size and structure must be a very important future direction. A significant challenge has to be faced: to produce better synthetic control, one may have to consider alternatives to the conventional carbon support materials. Many functional groups in these carbon supports cannot be easily controlled and have a significant effect on the Pt nanoparticle size and structure.

The present method to make carbon supports is not controllable. New carbon materials with clear frameworks and well-defined structures (including molecular structures and porous structures) must be used. Graphene is such a kind of new carbon material.<sup>135,136</sup> However, there is still no ideal graphene commercially available. Many defects or impurities exist in the graphene from present fabrication methods. In this regard, one may consider some novel carbon precursors, such as porous organic polymers.<sup>137,138</sup> Under certain carbonization conditions, a well-defined carbon support could be available in the near future.<sup>137</sup> Right now, the well-defined synthesis of platinum NPs is available.<sup>56,139</sup> If a well-defined carbon support with a designable, high surface area, desired porous structure, designable high conductivity and controllable anti-corrosion becomes available, it would be very helpful for an understanding of the ORR mechanism and for practical applications. (4) Among the various Pt based catalysts exploited, shell-core Pt NPs show the most significant potential as ORR catalysts because of their balance between activity and stability. The bulk production of this kind of Pt based catalyst is a significant challenge. (5) The nucleation and crystal growth of the Pt NPs has to be further investigated. The reduction methodology and the reducing agent have a remarkable influence on the nucleation of Pt NPs. However, the thermodynamics and kinetics of the nucleation of Pt NPs are still not clear. Normally, a slow nucleation occurs with the thermal and chemical reduction. This induces a difficulty in the size and structure control. Recently, a room temperature electron reduction has been employed to induce the fast nucleation of noble metal NPs.<sup>93,140,141</sup> The obtained Pt and other noble metal NPs always show the (111) plane as their principal facet.<sup>93,141</sup> Such an electron-reduced Pt/C catalyst has shown enhanced activity and stability for the ORR.<sup>93</sup> (6) *In situ* catalyst characteristics are still not available for ORR studies. The detection of chemical intermediates is still impossible, which makes the mechanism study very difficult. In this regard, theoretical investigations, such as DFT studies, are becoming more and more useful, with significant progress in computational catalysis. To conduct these, a well-defined carbon support is obviously very important. (7) Any progresses in *in situ* characterization and real-time detection technologies will contribute significantly to the design and synthesis of ORR catalysts. Some efforts have been made. For example, Becknell *et al.*<sup>29</sup> used X-ray absorption spectroscopy (XAS) as an *in situ* technique to study Pt<sub>3</sub>Ni nanoframe particles. Malacrida *et al.*<sup>18</sup> followed various steps of the electrochemical dealloying of Pt<sub>x</sub>Y NPs by *in situ* ambient pressure X-ray photoelectron spectroscopy (APXPS). Considering the effect of reactant and product species and Pt particle interaction in an acidic electrolyte, Chen and Kucernak<sup>40</sup> investigated ORR using single-Pt-particle electrodes of submicrometer dimensions, which can determine the sole effect of Pt particle size or facet. Recently an approach based on scanning electrochemical microscopy (SECM) for the study of geometric parameters and electrocatalytic activity of individual Pt NPs was developed by Kim *et al.*<sup>36</sup> The size, shape, spatial orientation and catalytic activity of Pt NPs could be determined at an individual level in nanoscale SECM where imaging was accompanied by theoretical modelling and

1 analysis. However, in the above measurements, Pt particles were  
2 on the scale of 60–120 nm (single-Pt-particle electrodes)<sup>40</sup> and  
3 50 nm to 5  $\mu\text{m}$  (SECM),<sup>36</sup> which are at least ten times bigger than  
4 the real Pt electrocatalyst size. Further improvements in these *in*  
5 *situ* characterizations of carbon-supported Pt catalysts can be  
6 expected. (8) Active carbon supports show a very large surface  
7 area and good conductivity and their application as Pt electro-  
8 catalyst supports has brought great progress in fuel cell tech-  
9 nology. However, carbon corrosion and their weak interaction  
10 with Pt NPs affect the stability and durability of Pt electro-  
11 catalysts. Carbon graphitisation,<sup>129</sup> decoration with oxides<sup>113</sup>  
12 and protective measures<sup>131–134</sup> are adopted for increasing carbon  
13 stability. The challenge is that the present support materials can  
14 hardly meet all of the requirements at the same time,<sup>130</sup> there-  
15 fore a comprehensive solution is expected to balance the surface  
16 area, conductivity, electrochemical stability and interaction  
17 with Pt NPs.

## 20 Acknowledgements

This work was supported by the European Commission's Marie  
21 Skłodowska-Curie Individual Fellowships (IF-EF) (H2020-MSCA-  
22 IF-2014, Grant no. 658217) and the National Natural Science  
23 Foundation of China (Grant no. 21476157  91334206).

## 24 Notes and references

- 1 T. Y. Ma, Y. Zheng, S. Dai, M. Jaroniec and S. Z. Qiao, *J. Mater. Chem. A*, 2014, **2**, 8676.
- 2 J. Kibsgaard, Y. Gorlin, Z. Chen and T. F. Jaramillo, *J. Am. Chem. Soc.*, 2012, **134**, 7758.
- 3 L. Su, W. Jia, C. M. Li and Y. Lei, *ChemSusChem*, 2014, **7**, 361.
- 4 M. Li, Z. Zhao, T. Cheng, A. Fortunelli, C.-Y. Chen, R. Yu, Q. Zhang, L. Gu, B. Merinov, Z. Lin, E. Zhu, T. Yu, Q. Jia, J. Guo, L. Zhang, W. A. Goddard III, Y. Huang and X. Duan, *Science*, 2016, **354**, 1414.
- 5 M. Shao, Q. Chang, J. P. Dodelet and R. Chenitz, *Chem. Rev.*, 2016, **116**, 3594.
- 6 J. K. Nørskov, J. Rossmeisl, A. Logadottir, L. Lindqvist, J. R. Kitchin, T. Bligaard and H. Jonsson, *J. Phys. Chem. B*, 2004, **108**, 17886.
- 7 M. K. Debe, *Nature*, 2012, **486**, 43.
- 8 G. Wu, K. L. More, C. M. Johnston and P. Zelenay, *Science*, 2011, **332**, 443.
- 9 A. Kongkanand and M. F. Mathias, *J. Phys. Chem. Lett.*, 2016, **7**, 1127.
- 10 C. R. Raj, A. Samanta, S. H. Noh, S. Mondal, T. Okajima and T. Ohsaka, *J. Mater. Chem. A*, 2016, **4**, 11156.
- 11 N. Jung, D. Y. Chung, J. Ryua, S. J. Yoo and Y. E. Sung, *Nano Today*, 2014, **9**, 433.
- 12 J. Luo, J. Yin, R. Loukrakpam, B. N. Wanjala, B. Fang, S. Shan, L. Yang, M. Nie, M. S. Ng, J. Kinzler, Y. S. Kim, K. K. Luo and C. J. Zhong, *J. Electroanal. Chem.*, 2013, **688**, 196.
- 13 J. Wang, B. Li, T. Yersak, D. Yang, Q. Xiao, J. Zhang and C. Zhang, *J. Mater. Chem. A*, 2016, **4**, 11559.

- 14 M. Escudero-Escribano, P. Malacrida, M. H. Hansen, U. G. Vej-Hansen, A. Velázquez-Palenzuela, V. Tripkovic, J. Schiøtz, J. Rossmeisl, I. E. L. Stephens and I. Chorkendorff, *Science*, 2016, **352**, 73.
- 15 S. Zhang, Y. Shao, G. Yin and Y. Lin, *J. Mater. Chem. A*, 2013, **1**, 4631.
- 16 Y. Bing, H. Liu, L. Zhang, D. Ghosh and J. Zhang, *Chem. Soc. Rev.*, 2010, **39**, 2184.
- 17 V. R. Stamenkovic, B. Fowler, B. S. Mun, G. Wang, P. N. Ross, C. A. Lucas and N. M. Markovic, *Science*, 2007, **315**, 493.
- 18 P. Malacrida, M. Escudero-Escribano, A. Verdagué-Casadevall, I. E. L. Stephens and I. Chorkendorff, *J. Mater. Chem. A*, 2014, **2**, 4234.
- 19 P. Malacrida, H. G. Sanchez Casalongue, F. Masini, S. Kaya, P. Hernández-Fernández, D. Deiana, H. Ogasawara, I. E. L. Stephens, A. Nilsson and I. Chorkendorff, *Phys. Chem. Chem. Phys.*, 2015, **17**, 28121.
- 20 C. Gümeçci, D. U. Cearnaigh, D. J. Casadonte Jr and C. Korzeniewski, *J. Mater. Chem. A*, 2013, **1**, 2322.
- 21 V. R. Stamenkovic, B. S. Mun, M. Arenz, K. J. J. Mayrhofer, C. A. Lucas, G. Wang, P. N. Ross and N. M. Markovic, *Nat. Mater.*, 2007, **6**, 241.
- 22 R. Zhao, Y. Liu, C. Liu, G. Xu, Y. Chen, Y. Tang and T. Lu, *J. Mater. Chem. A*, 2014, **2**, 20855.
- 23 M. B. Vukmirovic, J. Zhang, K. Sasaki, A. U. Nilekar, F. Uribe, M. Mavrikakis and R. R. Adzic, *Electrochim. Acta*, 2007, **52**, 2257.
- 24 M. A. Matin, J. H. Jang and Y. U. Kwon, *Int. J. Hydrogen Energy*, 2014, **39**, 3710.
- 25 Y. H. Chung, D. Y. Chung, N. Jung, H. Y. Park, Y. E. Sung and S. J. Yoo, *Int. J. Hydrogen Energy*, 2014, **39**, 14751.
- 26 Y. Nie, L. Li and Z. Wei, *Chem. Soc. Rev.*, 2015, **44**, 2168.
- 27 D. Raciti, J. Kubal, C. Ma, M. Barclay, M. Gonzalez, M. Chi, J. Greeley, K. L. More and C. Wang, *Nano Energy*, 2016, **20**, 202.
- 28 K. Sasaki, N. Marinkovic, H. S. Isaacs and R. R. Adzic, *ACS Catal.*, 2016, **6**, 69.
- 29 N. Becknell, Y. Kang, C. Chen, J. Resasco, N. Kornienko, J. Guo, N. M. Markovic, G. A. Somorjai, V. R. Stamenkovic and P. Yang, *J. Am. Chem. Soc.*, 2015, **137**, 15817.
- 30 C. H. Choi, M. Kim, H. C. Kwon, S. J. Cho, S. Yun, H. T. Kim, K. J. J. Mayrhofer, H. Kim and M. Choi, *Nat. Commun.*, 2016, **7**, 10922.
- 31 S. Chen, H. A. Gasteigera, K. Hayakawa, T. Tadac and Y. Shao-Horn, *J. Electrochem. Soc.*, 2010, **157**, A82.
- 32 M. J. Eslamibidgoli, J. Huang, T. Kadyk, A. Malek and M. Eikerling, *Nano Energy*, 2016, DOI: [10.1016/j.nanoen.2016.06.004i](https://doi.org/10.1016/j.nanoen.2016.06.004i) 
- 33 J. A. Keith, G. Jerkiewicz and T. Jacob, *ChemPhysChem*, 2010, **11**, 2779.
- 34 M. Markiewicz, C. Zalitis and A. Kucernak, *Electrochim. Acta*, 2015, **179**, 126.
- 35 L. W. Liao, Y. L. Zheng, J. Wei and Y. X. Chen, *Electrochem. Commun.*, 2015, **58**, 73.
- 36 J. Kim, C. Renault, N. Nioradze, N. Arroyo-Currás, K. C. Leonard and A. J. Bard, *J. Am. Chem. Soc.*, 2016, **138**, 8560.

- 1 37 J. Yue, Z. Du and M. Shao, *J. Phys. Chem. Lett.*, 2015, **6**, 3346.
- 38 H. S. Wroblowa and G. Razumney, *J. Electroanal. Chem.*, 1976, **69**, 195.
- 5 39 R. M. Felix-Navarro, M. Beltran-Gastelum, E. A. Reynoso-Soto, F. Paraguay-Delgado, G. Alonso-Nuñez and J. R. Flores-Hernandez, *Renewable Energy*, 2016, **87**, 31.
- 40 S. Chen and A. Kucernak, *J. Phys. Chem. B*, 2004, **108**, 3262.
- 41 M. J. Janik, C. D. Taylor and M. Neurock, *J. Electrochem. Soc.*, 2009, **156**, B126.
- 10 42 D. Eberle and B. Horstmann, *Electrochim. Acta*, 2014, **137**, 714.
- 43 M. P. Hyman and J. W. Medlin, *J. Phys. Chem. B*, 2005, **109**, 6304.
- 15 44 I. Katsounaros, W. B. Schneider, J. C. Meier, U. Benedikt, P. U. Biedermann, A. A. Auera and K. J. J. Mayrhofer, *Phys. Chem. Chem. Phys.*, 2012, **14**, 7384.
- 45 A. Nagoya, R. Jinnouchi, K. Kodama and Y. Morimoto, *J. Electroanal. Chem.*, 2015, **757**, 116.
- 20 46 Y. Sha, T. H. Yu, Y. Liu, B. V. Merinov and W. A. Goddard III, *J. Phys. Chem. Lett.*, 2010, **1**, 856.
- 47 R. F. de Morais, A. A. Franco, P. Sautet and D. Loffreda, *ACS Catal.*, 2015, **5**, 1068.
- 25 48 A. M. Gómez-Marin, R. Rizo and J. M. Feliu, *Catal. Sci. Technol.*, 2014, **4**, 1685.
- 49 T. Zhang and A. B. Anderson, *Electrochim. Acta*, 2007, **53**, 982.
- 50 J. L. Gavartin, M. Sarwar, D. C. Papageorgopoulos, D. Gunn, S. Garcia, A. Perlov, A. Krzystala, D. L. Ormsby, D. Thompsett, G. Goldbeck-Wood, A. Andersen and S. French, *ECS Trans.*, 2009, **25**, 1335.
- 30 51 Y. Sha, T. H. Yu, B. V. Merinov, P. Shirvanian and W. A. Goddard, *J. Phys. Chem. C*, 2012, **116**, 21334.
- 52 I. E. L. Stephens, A. S. Bondarenko, F. J. P. Alonso, F. Calle-Vallejo, L. Bech, T. P. Johansson, A. K. Jepsen, R. Frydendal, B. P. Knudsen, J. Rossmeisl and I. Chorkendorff, *J. Am. Chem. Soc.*, 2011, **133**, 5485.
- 35 53 M. Shao, A. Peles and K. Shoemaker, *Nano Lett.*, 2011, **11**, 3714.
- 40 54 T. Yu, D. Y. Kim, H. Zhang and Y. Xia, *Angew. Chem., Int. Ed.*, 2011, **50**, 2773.
- 55 S. Stolbov and M. A. Ortigoza, *J. Phys. Chem. Lett.*, 2012, **3**, 463.
- 45 56 J. Chen, B. Lim, E. P. Lee and Y. Xia, *Nano Today*, 2009, **4**, 81.
- 57 N. Tian, Z. Y. Zhou, S. G. Sun, Y. Ding and Z. L. Wang, *Science*, 2007, **316**, 732.
- 58 Y. Xia, Y. Xiong, B. Lim and S. E. Skrabalak, *Angew. Chem., Int. Ed.*, 2009, **48**, 60.
- 50 59 H. Y. Park, D. S. Yang, D. Bhattacharjya, M. Y. Song and J. S. Yu, *Int. J. Hydrogen Energy*, 2014, **39**, 1688.
- 60 H. Meng, Y. Zhan, D. Zeng, X. Zhang, G. Zhang and F. Jaouen, *Small*, 2015, **11**, 3377.
- 55 61 D. van der Vliet, C. Wang, M. Debe, R. Atanasoski, N. M. Markovic and V. R. Stamenkovic, *Electrochim. Acta*, 2011, **56**, 8695.
- 62 A. Chen and P. Holt-Hindle, *Chem. Rev.*, 2010, **110**, 3767.
- 63 D. H. Jung, S. J. Bae, S. J. Kim, K. S. Nahm and P. Kim, *Int. J. Hydrogen Energy*, 2011, **36**, 9115.
- 64 N. Todoroki, T. Dasai, Y. Asakimori and T. Wadayama, *J. Electroanal. Chem.*, 2014, **724**, 15.
- 65 J. Speder, I. Spanos, A. Zana, J. J. K. Kirkensgaard, K. Mortensen, L. Altmann, M. Bäumer and M. Arenz, *Surf. Sci.*, 2015, **631**, 278.
- 5 66 T. S. Ahmadi, Z. L. Wang, T. C. Green, C. Travis, A. Henglein and M. A. El-Sayed, *Science*, 1996, **272**, 1924.
- 67 M. Inaba, M. Ando, A. Hatanaka, A. Nomoto, K. Matsuzawa, A. Tasaka, T. Kinumoto, Y. Iriyama and Z. Ogumi, *Electrochim. Acta*, 2006, **52**, 1632.
- 10 68 D. Y. Wang, H. L. Chou, C. C. Cheng, Y. H. Wu, C. M. Tsai, H. Y. Lin, Y. L. Wang, B. J. Hwang and C. C. Chen, *Nano Energy*, 2015, **11**, 631.
- 69 W. A. Egli, A. Visintin, W. E. Triaca and A. J. Arvia, *Appl. Surf. Sci.*, 1993, **68**, 583.
- 15 70 S. Sun, D. Yang, G. Zhang, E. Sacher and J. P. Dodelet, *Chem. Mater.*, 2007, **19**, 6376.
- 71 S. Sun, D. Yang, D. Villers, G. Zhang, E. Sacher and J. P. Dodelet, *Adv. Mater.*, 2008, **20**, 571.
- 20 72 Y. Lu, S. Du and R. Steinberger-Wilckens, *Appl. Catal., B*, 2015, **164**, 389.
- 73 S. Sun, F. Jaouen and J. P. Dodelet, *Adv. Mater.*, 2008, **20**, 3900.
- 25 74 B. Li, Z. Yan, D. C. Higgins, D. Yang, Z. Chen and J. Ma, *J. Power Sources*, 2014, **262**, 488.
- 75 L. Bu, Y. Feng, J. Yao, S. Guo, J. Guo and X. Huang, *Nano Res.*, 2016, **9**, 2811.
- 30 76 X. Yao, K. Su, S. Sui, L. Mao, A. He, J. Zhang and S. Du, *Int. J. Hydrogen Energy*, 2013, **38**, 12374.
- 77 K. Su, X. Yao, S. Sui, Z. Wei, J. Zhang and S. Du, *Fuel Cells*, 2015, **15**, 449.
- 78 K. Su, X. Yao, S. Sui, Z. Wei, J. Zhang and S. Du, *Int. J. Hydrogen Energy*, 2014, **39**, 3219.
- 35 79 K. Su, S. Sui, X. Yao, Z. Wei, J. Zhang and S. Du, *Int. J. Hydrogen Energy*, 2014, **39**, 3397.
- 80 Z. Wei, K. Su, S. Sui, A. He and S. Du, *Int. J. Hydrogen Energy*, 2015, **40**, 3068.
- 81 Z. Wei, A. He, K. Su and S. Sui, *J. Energy Chem.*, 2015, **24**, 213.
- 40 82 C. Huang, C. B. Odetola and M. Rodgers, *Appl. Catal., A*, 2015, **499**, 55.
- 83 T. Y. Jeon, S. J. Yoo, Y. H. Cho, S. H. Kang and Y. U. Sung, *Electrochem. Commun.*, 2010, **12**, 1796.
- 45 84 R. K. Ahluwalia, X. Wang, A. Lajunen, A. J. Steinbach, S. M. Hendricks, M. J. Kurkowski and M. K. Debe, *J. Power Sources*, 2012, **215**, 77.
- 85 W. Shimizu, K. Okada, Y. Fujita, S. S. Zhao and Y. Murakami, *J. Power Sources*, 2012, **205**, 24.
- 50 86 H. J. Kim, Y. S. Kim, M. H. Seo, S. M. Choi, J. Cho, G. W. Huber and W. B. Kim, *Electrochem. Commun.*, 2010, **12**, 32.
- 87 Z. Niu, N. Becknell, Y. Yu, D. Kim, C. Chen, N. Kornienko, G. A. Somorjai and P. Yang, *Nat. Mater.*, 2016, **15**, 1188.
- 55 88 A. Dhand, R. O'Hayre and H. Pitsch, *ECS Trans.*, 2008, **16**, 1131.
- 89 K. Kinoshita, *J. Electrochem. Soc.*, 1990, **137**, 845.
- 90 J. Hu, L. Wu, K. A. Kuttiyiel, K. R. Goodman, C. Zhang, Y. Zhu, M. B. Vukmirovic, M. G. White, K. Sasaki and R. R. Adzic, *J. Am. Chem. Soc.*, 2016, **138**, 9294.

- 1 91 W. H. Lee and H. Kim, *Int. J. Hydrogen Energy*, 2013, **38**, 7126.
- 92 H. Yano, M. Kataoka, H. Yamashita, H. Uchida and M. Watanabe, *Langmuir*, 2007, **23**, 6438.
- 5 93 W. Wang, Z. Wang, M. Yang, C. J. Zhong and C. J. Liu, *Nano Energy*, 2016, **25**, 26.
- 94 H. Yano, M. Watanabe, A. Iiyama and H. Uchida, *Nano Energy*, 2016, **29**, 323.
- 10 95 N. E. Sahin, T. W. Napporn, L. Dubau, F. Kadirgan, J.-M. Léger and K. B. Kokoh, *Appl. Catal., B*, 2017, **203**, 72.
- 96 H. Y. Park, T. Y. Jeon, J. H. Jang, S. J. Yoo, K. H. Choi, N. Jung, Y. H. Chung, M. Ahn, Y. H. Cho, K. S. Lee and Y. E. Sung, *Appl. Catal., B*, 2013, **129**, 375.
- 15 97 C. Zhang, S. Y. Hwang and Z. Peng, *J. Mater. Chem. A*, 2014, **2**, 19778.
- 98 D. Li, C. Wang, D. S. Strmcnik, D. V. Tripkovic, X. Sun, Y. Kang, M. Chi, J. D. Snyder, D. van der Vliet, Y. Tsai, V. R. Stamenkovic, S. Sun and N. M. Markovic, *Energy Environ. Sci.*, 2014, **7**, 4061.
- 20 99 W. Sheng, S. Chen, E. Vescovo and Y. Shao-Horn, *J. Electrochem. Soc.*, 2012, **159**, B96.
- 100 M. Inaba, M. Ando, A. Hatanaka, A. Nomoto, K. Matsuzawa, A. Tasaka, T. Kinumoto, Y. Iriyama and Z. Ogumi, *Electrochim. Acta*, 2006, **52**, 1632.
- 25 101 M. C. S. Escaño, *Nano Res.*, 2015, **8**, 1689.
- 102 H. Shi, S. M. Auerbach and A. Ramasubramaniam, *J. Phys. Chem. C*, 2016, **120**, 11899.
- 103 S. C. Roy, A. W. Harding, A. E. Russell and K. M. Thomas, *J. Electrochem. Soc.*, 1997, **144**, 2323.
- 30 104 E. Auer, A. Freund, J. Pietsch and T. Tacke, *Appl. Catal., A*, 1998, **173**, 259.
- 105 S. Y. Huang, P. Ganesan, S. Park and B. N. Popov, *J. Am. Chem. Soc.*, 2009, **131**, 13898.
- 35 106 M. Uchida, Y. Fukuoka, Y. Sugawara, N. Eda and A. Ohta, *J. Electrochem. Soc.*, 1996, **143**, 2245.
- 107 Y.-C. Park, H. Tokiw, K. Kakinuma, M. Watanabe and M. Uchid, *J. Power Sources*, 2016, **315**, 179.
- 40 108 S. Malik, L. Smith, J. Sharman, E. M. Holt and S. P. Rigby, *Ind. Eng. Chem. Res.*, 2016, **55**, 10850.
- 109 H. S. Kim, Y. Lee, J. G. Lee, H. J. Hwang, J. Jang, S. M. Juon, A. Dorjgotov and Y. G. Shul, *Electrochim. Acta*, 2016, **193**, 191.
- 45 110 N. Jung, S. M. Kim, D. H. Kang, D. Y. Chung, Y. S. Kang, Y. H. Chung, Y. W. Choi, C. Pang, K. Y. Suh and Y. E. Sung, *Chem. Mater.*, 2013, **25**, 1526.
- 111 A. Ueda, Y. Yamada, T. Ioroi, N. Fujiwara, K. Yasuda, Y. Miyazaki and T. Kobayashi, *Catal. Today*, 2003, **84**, 223.
- 50 112 O. A. Baturina, Y. Garsany, T. J. Zega, R. M. Stroud, T. Schull and K. E. Swider-Lyons, *J. Electrochem. Soc.*, 2008, **155**, B1314.
- 113 T. Masuda, H. Fukumitsu, K. Fugane, H. Togasaki, D. Matsumura, K. Tamura, Y. Nishihata, H. Yoshikawa, K. Kobayashi, T. Mori and K. Uosaki, *J. Phys. Chem. C*, 2012, **116**, 10098.
- 55 114 Y. P. Xiao, W. J. Jiang, S. Wan, X. Zhang, J. S. Hu, Z. D. Wei and L. J. Wan, *J. Mater. Chem. A*, 2013, **1**, 7463.
- 115 S. Du, Y. Lu, S. K. Malladi, Q. Xu and R. Steinberger-Wilckens, *J. Mater. Chem. A*, 2014, **2**, 692.
- 116 Z. Liu, Q. Shi, R. Zhang, Q. Wang, G. Kang and F. Peng, *J. Power Sources*, 2014, **268**, 171.
- 117 C. Gupta, P. H. Maheshwari, D. Sachdev, A. K. Sahud and S. R. Dhakate, *RSC Adv.*, 2016, **6**, 32258.
- 118 D. Higgins, P. Zamani, A. Yu and Z. Chen, *Energy Environ. Sci.*, 2016, **9**, 357.
- 119 B. P. Vinayan, R. Nagar and S. Ramaprabhu, *J. Mater. Chem.*, 2012, **22**, 25325.
- 120 L. T. Soo, K. S. Loha, A. B. Mohamad, W. R. W. Daud and W. Y. Wong, *Appl. Catal., A*, 2015, **497**, 198.
- 121 Y. Tian, Y.-J. Liu, J.-X. Zhao and Y.-H. Ding, *RSC Adv.*, 2015, **5**, 34070.
- 122 J. I. Paredes, S. Villar-Rodil, A. Martínez-Alonso and J. M. D. Tascín, *Langmuir*, 2008, **24**, 10560.
- 123 V. B. Parambath, R. Nagar, K. Sethupathi and S. Ramaprabhu, *J. Phys. Chem. C*, 2011, **115**, 15679.
- 124 L. Xin, F. Yang, S. Rasouli, Y. Qiu, Z.-F. Li, A. Uzunoglu, C.-J. Sun, Y. Liu, P. Ferreira, W. Li, Y. Ren, L. A. Stanciu and J. Xie, *ACS Catal.*, 2016, **6**, 2642.
- 20 125 R. Wang, D. C. Higgins, M. A. Hoque, D. Lee, F. Hassan and Z. Chen, *Sci. Rep.*, 2013, **3**, 2431.
- 126 J. H. Kim, J. Y. Cheon, T. J. Shin, J. Y. Park and S. H. Joo, *Carbon*, 2016, **101**, 449.
- 127 S. V. Selvaganesh, P. Sridhar, S. Pitchumani and A. K. Shukla, *J. Electrochem. Soc.*, 2012, **160**, F49.
- 128 S.-M. Kim, Y.-K. Heo, K.-T. Bae, Y.-T. Oh, M.-H. Lee and S.-Y. Lee, *Carbon*, 2016, **101**, 420.
- 129 J. C. Meier, C. Galeano, I. Katsounaros, J. Witte, H. J. Bongard, A. A. Topalov, C. Baldizzone, S. Mezzavilla, F. Schüth and K. J. J. Mayrhofer, *Beilstein J. Nanotechnol.*, 2014, **5**, 44.
- 30 130 X. X. Wang, Z. H. Tan, M. Zeng and J. N. Wang, *Sci. Rep.*, 2014, **4**, 4437.
- 131 M. R. Berber, I. H. Hafez, T. Fujigaya and N. Nakashima, *Sci. Rep.*, 2015, **5**, 16711.
- 35 132 K. Yoshii, K. Yamaji, T. Tsuda, H. Matsumoto, T. Sato, R. Izumi, T. Torimoto and S. Kuwabata, *J. Mater. Chem. A*, 2016, **4**, 12152.
- 133 Y. Luo, L. Calvillo, C. Daiguebonne, M. K. Daletou, G. Granozzi and N. Alonso-Vante, *Appl. Catal., B*, 2016, **189**, 39.
- 40 134 Y. Li, H. Xu, H. Zhao, L. Lu and X. Sun, *J. Appl. Electrochem.*, 2016, **46**, 183.
- 135 I. Lee, J. B. Joo and M. Shokouhimehr, *Chin. J. Catal.*, 2015, **36**, 1799.
- 45 136 J. Duan, S. Chen, M. Jaroniec and S. Z. Qiao, *ACS Catal.*, 2015, **5**, 5207.
- 137 Z.-A. Huang, C. Chen, X.-D. Yang, X.-B. Fan, W. Zhou, C.-H. Tung, L.-Z. Wu and H. Cong, *J. Am. Chem. Soc.*, 2016, **138**, 11144.
- 50 138 Y. Zhou, Z. H. Xiang, D. P. Cao and C.-J. Liu, *Chem. Commun.*, 2013, **49**, 5633.
- 139 D. S. He, D. P. He, J. Wang, Y. Lin, P. Q. Yin, X. Hong, Y. Wu and Y. D. Li, *J. Am. Chem. Soc.*, 2016, **138**, 1494.
- 55 140 Z. Y. Wang, M. Y. Li, W. Wang, M. Fang, Q. D. Sun and C. J. Liu, *Nano Res.*, 2016, **9**, 1148.
- 141 Y.-X. Pan, H.-P. Cong, Y.-L. Men, S. Xin, Z.-Q. Sun, C.-J. Liu and S.-H. Yu, *ACS Nano*, 2015, **9**, 11258.